AGU PUBLICATIONS

Paleoceanography

RESEARCH ARTICLE
10.1002/2014PA002705

Key Points:
- Planktic foraminifer assemblages and size properties in the SE Mediterranean
- Change of hydrology from monsoon-driven to NAO-controlled system from 6.4 ka
- Intensification of the influence of NAO and teleconnections from 2.9 ka

Correspondence to:
M. Mojtahid,
meryem.mojtahid@univ-angers.fr

Citation:
Mojtahid, M., R. Manceau, R. Schiebel, R. Hennekam, and G. J. de Lange (2015), Thirteen thousand years of southeastern Mediterranean climate variability inferred from an integrative planktic foraminiferal-based approach, *Paleoceanography*, *30*, 402–422, doi:10.1002/2014PA002705.

Received 29 AUG 2014
Accepted 16 MAR 2015
Accepted article online 23 MAR 2015
Published online 29 APR 2015

Thirteen thousand years of southeastern Mediterranean climate variability inferred from an integrative planktic foraminiferal-based approach

Meryem Mojtahid[1], Rose Manceau[1,2], Ralf Schiebel[1], Rick Hennekam[3], and Gert J. de Lange[3]

[1]LPG-BIAF UMR-CNRS 6112, University of Angers, UFR Sciences, Angers, France, [2]Now at College of Physical and Mathematical Sciences, Australian National University, Canberra, ACT, Australia, [3]Department of Earth Sciences-Geochemistry, Faculty of Geosciences, Utrecht University, Utrecht, Netherlands

Abstract Over the past 13 ka, the hydrology for the southeastern Mediterranean was mainly regulated by Nile River runoff, which in turn was controlled by climate forcing. Being affected by orbital forcing, and the position of the Intertropical Convergence Zone (ITCZ), planktic foraminiferal data (assemblages, stable isotopes, and size properties) indicate three major periods. (1) From 13.0 to 11.5 ka, the upper water column was well-mixed, cold, and productive. (2) From 11.5 to 6.4 ka, hydrology and foraminifers were affected by intensified monsoonal circulation. The enhanced size of *Globigerinoides ruber* is interpreted as a response to environmental stress caused by low-saline waters. (3) After 6.4 ka, the southward retreat of the ITCZ caused a decrease in freshwater discharge and hence a return to ecological equilibrium. A drop in foraminifer diversity from 2.9 to 1.1 ka was related to more arid conditions, and limited supply of nutrients from the Nile River. We suggest a link to a negative North Atlantic Oscillation (NAO) marking the Roman Humid Period in the western Mediterranean, and in anti-phase with the southeastern Mediterranean aridity. Because Nile River runoff exerted major control on surface hydrology, a connection to Indian and Pacific climate systems partially controlling precipitation over the Nile catchment area is hypothesized. From 1.1 to 0.54 ka, high foraminifer diversity indicates humid conditions synchronous to the Medieval Climate Anomaly under a positive NAO state. Over the past 0.54 ka encompassing the Little Ice Age, another arid period is indicated by a drop in foraminifer diversity.

1. Introduction

The Levantine is currently experiencing increasing aridification [*IPCC*, 2013]. Historical climate change in the Levantine is well documented and of major interest since this fertile crescent is the cradle of our civilization [*Issar*, 2003]. Documentation of past natural climate variability, particularly during the Holocene, is needed to better understand the main drivers of such variability on human timescales. Various paleoclimate archives have been analyzed from the eastern Mediterranean, including continental (palynology) [e.g., *Bottema*, 1995; *Rossignol-Strick*, 1995; speleothems, e.g., *Bar-Matthews and Ayalon*, 2011; *Bar-Matthews et al*., 1998, 1999, 2003; *Orland et al*., 2012] and marine settings [e.g., *Rohling et al*., 1993, 2004; *Emeis et al*., 2000; *Schilman et al*., 2001, 2002, 2003; *Ducassou et al*., 2008; *Box et al*., 2011; *Revel et al*., 2014]. However, besides lake sediments and speleothems, few records resolve decadal to centennial timescales. Holocene records include time intervals of changing temperature and humidity in the eastern Mediterranean, which are thought to be linked to changes of high-latitude and low-latitude climate systems [e.g., *Bar-Matthews et al*., 2003; *Almogi-Labin et al*., 2009; *Revel et al*., 2010]. Yet their respective influence is not fully understood. A major episode of environmental change from ~10 to 6 cal ka B.P. (sapropel S1) was possibly linked to insolation-driven changes of the northeast African monsoon [e.g., *Rohling*, 1994]. This period is not only known as a humid climate period from continental archives but also as the most recent period during which distinct organic-rich sediments (sapropels) were deposited throughout the eastern Mediterranean [e.g., *De Lange et al*., 2008]. The deposition of sapropel S1 has been attributed to reduced ventilation. This was related to increased North African river runoff and precipitation over the Mediterranean, enhanced biological productivity resulting from enhanced nutrients supply, or a combination of both [e.g., *Rossignol-Strick et al*., 1982; *Rohling*, 1994; *Kallel et al*., 1997; *De Lange et al*., 2008].

Riverine mud belt deposits capture short-term climate variability, bearing continuous and expanded sedimentary successions and retaining both continental and marine environmental signals at high resolution through high sedimentation rates. The range of temporal variability in these archives spans from decadal to millennial scales,

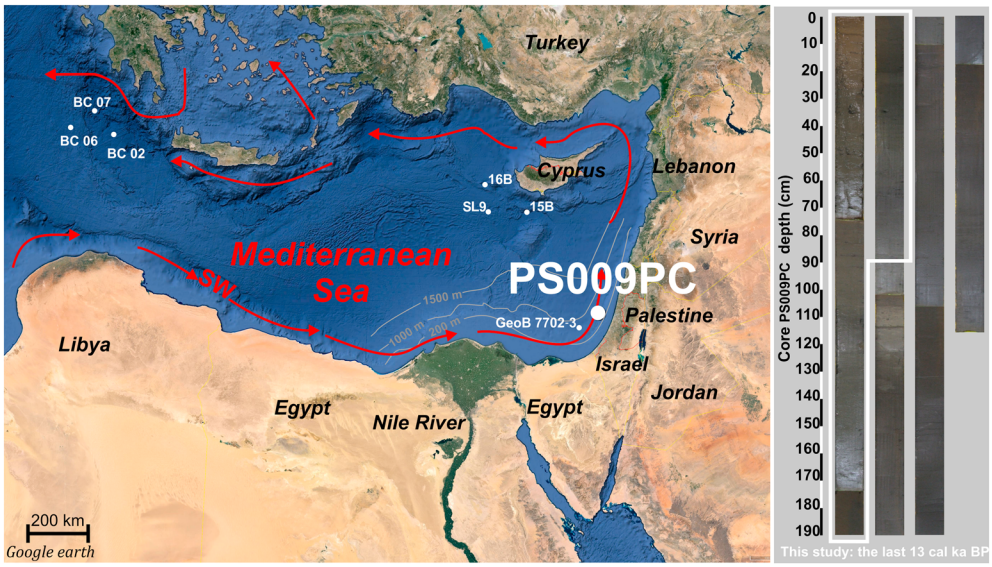

Figure 1. Core location PS009PC in the eastern Levantine Basin (32°07.7′N, 34°24.4′E; 552 m water depth). SW: Mediterranean Surface Waters. The red arrows show modern surface water circulation. The locations of other relevant studies are reported: 15B and 16B (planktic tows; *Pujol and Vergnaud-Grazzini* [1995]); SL9 (box core; *Principato et al.* [2006]); GeoB 7702-3 (gravity core; *Castañeda et al.* [2010]); BC02, BC06, and BC07 (box cores; *Principato et al.* [2003]).

allowing forcing factors to be investigated at different timescales. The present study focuses on the marine sediment core PS009PC located in the southeastern Levantine Basin (Figure 1). The area is known to be largely influenced by Nile River discharge [*Krom et al.*, 1999]. An average sedimentation rate of 33 cm/ka permits studying marine environmental variability at high resolution that could not be obtained by most other studies in the eastern Mediterranean [*Luz and Bernstein*, 1976; *Jorissen et al.*, 1993; *Capotondi et al.*, 1999; *Sbaffi et al.*, 2001; *Principato et al.*, 2003, 2006; *Rouis-Zargouni et al.*, 2010]. Core PS009PC was earlier studied for its inorganic geochemical properties (Ti/Al, Ba/Al, V/Al) and the oxygen isotope composition of the planktic foraminifer *Globigerinoides ruber* [*Hennekam and de Lange*, 2012; *Hennekam et al.*, 2014]. Our work uses the age model presented in the study of *Hennekam et al.* [2014] for an easier comparison with the published data from the same core. Our study discusses the planktic foraminifer assemblages and their morphometric properties as proxies of the surface water ecology in the region on centennial timescales. In general, the standing stock, composition, and size of planktic foraminifers observed at a specific time interval and location result from the interaction between biological, hydrological (e.g., temperature, turbidity, water column stratification, and salinity), and other ecological factors (e.g., food availability) [e.g., *Bé and Tolderlund*, 1971; *Bijma et al.*, 1990; *Schmidt et al.*, 2004a]. Each species might respond differently to one or more of those parameters depending on its depth habitat in the water column and the seasonal distribution. For instance, *Globigerinoides ruber* is a tropical-subtropical symbiont-bearing species generally inhabiting oligotrophic surface waters [*Bé and Tolderlund*, 1971]. However, by tolerating a larger salinity gradient than most other species [*Schmuker and Schiebel*, 2002], *G. ruber* may adapt to low-saline tropical-subtropical surface waters. Deep-dwelling species, such as *Globorotalia inflata*, are more likely to be influenced by other factors such as water column mixing. Size changes in planktic foraminifers are also indicative of ecological factors such as temperature [e.g., *Hecht*, 1976], upwelling intensity [*Naidu and Malmgren*, 1995], surface water stratification, and primary productivity [e.g., *Schmidt et al.*, 2004a].

The main objective of this study is to reconstruct the temporal variability of planktic ecosystems during the last 13 cal ka B.P. in the Levantine Basin at high resolution. Temporal variability is discussed for paleoclimate changes affecting Nile River discharge, Mediterranean thermohaline circulation, water column characteristics (sea surface temperatures, salinity, and turbidity), and surface productivity in response to various forcing factors.

2. Study Area

2.1. Core Location and Sediment Characteristics

The Levantine Basin is the easternmost part of the Mediterranean (Figure 1). Sediments are composed mainly of smectites [*Hamann et al.*, 2009] sourced from Nile River discharge with a flux estimated at 120×10^6 t a^{-1}

for the pre-Aswan modern times [*Revel et al*., 2010, and references therein]. Piston core PS009PC (32°07.7′N, 34°24.4′E, 552 m water depth, 690 cm length) was retrieved from a topographic elevation, thus avoiding possible turbidite pathways and effects of downslope transport [*Hennekam et al*., 2014] (Figure 1). Consequently, we do not record an increase in sedimentation rates during sapropel S1 deposition as being the case in settings in front of the Nile River [e.g., *Revel et al*., 2010]. Indeed, following the age model of *Hennekam et al*. [2014], sedimentation rates were stable from 13 to 6.6 cal ka B.P. (12 cm/ka). Around 6.6 cal ka B.P., sedimentation rates increased up to the core top, possibly caused by increased mass accumulation rates affected by gradually drier conditions and enhanced erosion in the Blue Nile source area [*Hennekam et al*., 2014].

2.2. Oceanographic Setting and Atmospheric Circulation

The southeastern Levantine Sea comprises three main water masses. (1) Modified Atlantic water (MAW; Figure 1) is in the surface 50–200 m [*UNEP/MAP*, 2012], originating from the Atlantic. This water mass increases in salinity with increasing evaporation to the east and reaches 38–39 PSU in the Levantine [*Wüst*, 1961; *Kress et al*., 2014]. Temperatures vary from ~17°C in winter to ~28°C in summer [*Marullo et al*., 1999]. Nile-derived sediments and freshwater are transported to our core location by the means of MAW. (2) The Levantine intermediate water (LIW) between 200 and 600 m water depth is characterized by temperatures of ~15.5°C and salinities of ~39.1 [*Kress et al*., 2014]. LIW is formed in the Rhodes gyre in winter, as a result of downwelling of the saline MAW after being cooled down by northern winds [*UNEP/MAP*, 2012]. (3) The eastern Mediterranean deep water, which fills up the deeper part of the basin, is cooler (~13.5°C) and less saline (~38.7) than the LIW [*Kress et al*., 2014]. Our core is mainly bathed in the LIW.

The Levantine Basin is affected by three main atmospheric systems: (1) the westerlies, (2) the subtropical high-pressure system, and (3) the monsoon system. In winter, intensification of Atlantic westerlies brings cold air masses to the Mediterranean [*Issar*, 2003]. While traveling over the warm Mediterranean Sea, air masses become saturated with moisture, which precipitates as rain and snow in the eastern Mediterranean [e.g., *Eshel*, 2002]. The impact of this system is fading toward the southeast. Summers are characterized by the strengthening of the Azores subtropical high causing hot and dry climate [*Gasse*, 2000] and deposition of Saharan dust [*Revel et al*., 2010]. In addition, the Nile River affects the eastern Mediterranean and particularly the Levantine Basin. Nile River runoff is related to the northeast African monsoon system. This atmospheric system controls the northward penetration of the Intertropical Convergence Zone (ITCZ), which in turn controls the runoff of the Nile River. This system is especially active from July to October [*Williams et al*., 2006]. Two potential moisture sources of the Nile River catchments are the Atlantic Ocean (Blue Nile/Ethiopian highlands) and the Atlantic/Indian system (White Nile/Lake Victoria) [*Hennekam et al*., 2014, and references therein]. Those two moisture sources have varied in response to past atmospheric variability [*Revel et al*., 2010, and references therein].

3. Material and Methods

Piston core PS009PC was recovered during the PASSAP cruise with the R/V *Pelagia* (5 May to 1 June 2000). The present study focuses on the upper 278 cm of the core covering the last 13 cal ka B.P. (Figure 1).

3.1. Age Model

The age model of core PS009PC is based on 11 ^{210}Pb and 7 ^{14}C data [*Hennekam et al*. 2014]. The ^{210}Pb analyses were performed on sediment samples of the corresponding box core PS008BC obtained from the same location as piston core PS009PC. PS008BC was subsequently correlated to PS009PC by using geochemical profiles [*Hennekam and de Lange*, 2012]. The ^{14}C analyses were performed on approximately 10 mg of planktic foraminifer tests of different species. Accelerator mass spectrometry ^{14}C ages were converted to calendar ages (years before present, B.P.) using the depositional model provided by OxCaL 4.1.7 [*Ramsey*, 2009] based on the Marine09 radiocarbon calibration curve [*Reimer et al*., 2009] after applying a 21 ± 60 year local reservoir correction [*Hennekam et al*., 2014 and references therein]. The mean error on ages is 42 ± 10 years for uncalibrated ^{14}C ages and 177 ± 20 cal years after calibration.

3.2. Foraminifer Assemblage Analyses

The upper 278 cm of core PS009PC was subsampled every 0.5 cm. All subsamples were washed through 150 μm and 63 μm sieves. Two consecutive samples were combined for foraminifer analyses to obtain

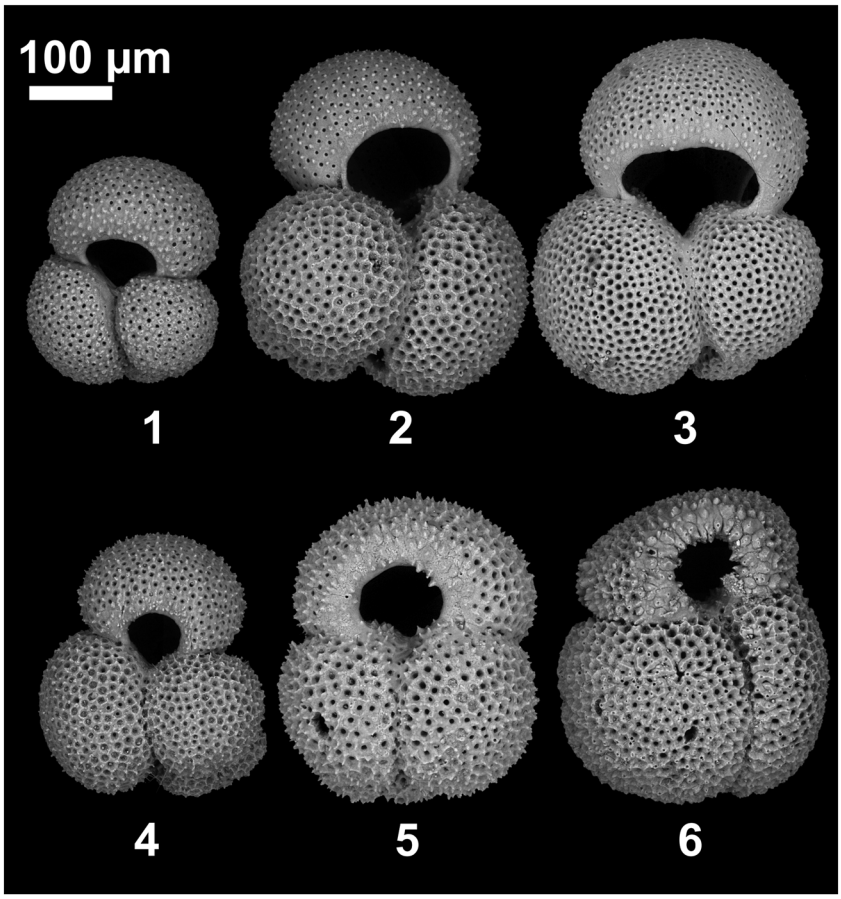

Plate 1. *Globigerinoides ruber* (white) morphotypes sensu stricto (s.s., images 1–3, upper row) and sensu lato (s.l., images 4–6, lower row) following the classification of *Wang* [2000]. Specimens 1–4 are from 170.1 cm and 5–6 from 189.7 cm core depth.

enough specimens at a resolution of 1 cm. The subsamples were wet weighed, and the dry weight was estimated using the sediment water content, which was derived by wet and dry weighing of parallel samples [*Hennekam and de Lange*, 2012]. Planktic foraminifer assemblages >150 µm were analyzed every 2 to 4 cm (78 samples; ~38 to 320 years). Samples were split, using a microsplitter when necessary. At least 300 specimens were picked and identified from a single split [*van der Plas and Tobi*, 1965]. Relative (percentages) and absolute abundances (number of individuals per gram of dry sediment; ind/g) of species and planktic foraminifer accumulation rates (PFAR, ind/cm^{2}ka) were calculated from

$$\mathrm{PFAR} = \mathrm{AA} \times \mathrm{SR} \times \mathrm{DBD}$$

with AA = absolute abundances, SR = sedimentation rate (cm/ka), and DBD = dry bulk density (g/cm^3).

Species were classified after *Bé and Tolderlund* [1971] and *Hemleben et al*. [1989]. The two morphotypes *Globigerinoides ruber* sensu stricto (s.s.) and sensu lato (s.l.) were distinguished following *Wang* [2000] (Plate 1). Foraminifer diversity was quantified using the Shannon index (entropy, *H*).

3.3. Stable Isotopes

The methodology used for stable isotope measurements is described in detail in *Hennekam et al*. [2014]. In short, stable oxygen and carbon isotopes were measured with a Finnigan MAT-253 mass spectrometer at the University of Utrecht, with a standard deviation of ±0.04‰ for δ^{13}C and ±0.06‰ for δ^{18}O obtained from 137 measurements of the NBS-19 standard. The δ^{13}C and δ^{18}O analyses were performed at 1 cm resolution (277 samples). Approximately 20–30 tests of *Globigerinoides ruber* (white) were handpicked from

the 250–300 μm fraction for samples below 173 cm core depth (~5.1 cal ka B.P.), and from the 212–300 μm fraction above 173 cm, to obtain sufficient *G. ruber* tests for measurements. The carbon isotope data were reported relative to the Vienna PeeDee Belemnite. The $\delta^{18}O$ data were previously published by *Hennekam et al.* [2014]. We specifically discuss $\delta^{13}C$ data in the present study.

3.4. Foraminifer Size Analyses

Morphometric analyses of the tests of both morphotypes of *Globigerinoides ruber* white s.s. (57 samples) and s.l. (54 samples) and *Orbulina universa* (53 samples) were performed using an automated incident light microscope Leica©Z16APO driven by analySIS® software [*Bollmann et al.*, 2004], installed at the University of Angers. Among the measured morphometric parameters, the minimum test diameter represents the size of the specimens [e.g., *Beer et al.*, 2010]. Even though *O. universa*, unlike *G. ruber*, was not a dominant species in any sample, its size variability in response to environmental parameters is better documented compared to other species [e.g., *Bé and Duplessy*, 1976; *Hecht*, 1976]. To be statistically accurate, some samples were combined to obtain at least 10 individuals of *O. universa*, and average sizes were calculated for these samples (Table 2).

4. Results

4.1. Absolute Abundances and Accumulation Rates

Absolute abundances and the PFAR ranged between ~1 ind/g and 1870 ind/g and between 40 ind/cm^{2}ka and 13762 ind/cm^{2}ka, respectively. The highest values occurred from ~10 to 5.5 cal ka B.P. with a return to background values at ~8.8 ka and low values at ~8.1 ka (Figure 2a).

4.2. Diversity and Relative Abundances

Highest Shannon diversity (*H*) occurred at ~12.6 cal ka B.P., during the mid-Holocene, and around 1.1–0.54 ka. Low *H* diversity marked the early Holocene (~10.8 ka), the first phase of sapropel S1a deposit at ~9.4 ka, and from ~2.9 to 1.1 ka (Figure 2b).

The major species found in core PS009PC are presented in Figure 2 and Table 1. *Globigerinoides ruber* accounted for an average of 64% of the total planktic foraminifer assemblage with maximum abundances between ~11.6 and 9.4 ka and minimum values around 12.6 ka and ~1.1–0.54 ka (Figure 2c). *Globigerinoides ruber* white was the most dominant type composing ~80% of the total *G. ruber*. *Globigerinoides ruber* white s.s. increased in dominance over *G. ruber* white s.l. after 6.4 ka. *Globigerinoides ruber* pink s.s. reached maximum relative values (~20%) around 0.3 ka, whereas it composed $<$5% in most samples. The three morphotypes of *Globigerinoides sacculifer* (*G. sacculifer* sac, *quadrilobatus*, and *trilobus*) covaried throughout record (Figure 2d). The species first occurred at ~11.7 ka, was absent from ~10.1 to 8.8 ka, and subsequently reappeared at $\leq$10%. The highest faunal parts of *G. sacculifer* (~25%) were recorded around 1.0 ka (Figure 2d). Maximum abundance of *Globigerina bulloides* (~30%) was recorded around 12 ka, and minimum numbers occurred from ~10.1 to 6.4 ka (Figure 2e). After 6.4 ka, *G. bulloides* accounted for ~5% of the assemblage except between 0.3 and 1.0 ka (~10%). *Neogloboquadrina pachyderma* and *Neogloboquadrina incompta* were rare except for maximum occurrences $>$10% around 12 ka and during the last 1.4 to 0.2 ka (Figure 2f). Deep-dwelling *G. inflata* and *Globorotalia truncatulinoides* were present at significant faunal parts only in the early record and for a short interval of time following 6.4 ka (*G. inflata* only) (Figure 2g).

4.3. Stable Carbon Isotopes

The stable carbon isotope values of *G. ruber* ($\delta^{13}C_{G.\ ruber}$) show four main phases throughout record (Figure 2h): (1) an increase from 13.0 to 11.0 cal ka B.P. from 0.56 to 1.25‰, then overall stable values until ~11 cal ka B.P.; (2) a shift to values as low as ~0.03‰ from 11.0 to 10.2 ka; (3) a general increase from ~10.2 to 6.0 ka to reach ~1.13‰; and (4) a decrease of $\delta^{13}C_{G.\ ruber}$ from 1.13‰ at ~6.0 ka to 0.9‰ at 1.8 ka, followed by a steep decrease to 0.5‰ at the top of core.

4.4. Test Size Analyses

Globigerinoides ruber white s.s. and s.l. showed similar size evolution along record (Figure 3). At 13–11.5 cal ka B.P., average minimal diameters of both morphotypes s.s. and s.l. were 223 ± 4 μm and 283 ± 12 μm, respectively. At the start of the Holocene, both morphotypes significantly increased in size to 375 ± 6 μm (s.s.) and 467 ± 11 μm (s.l.)

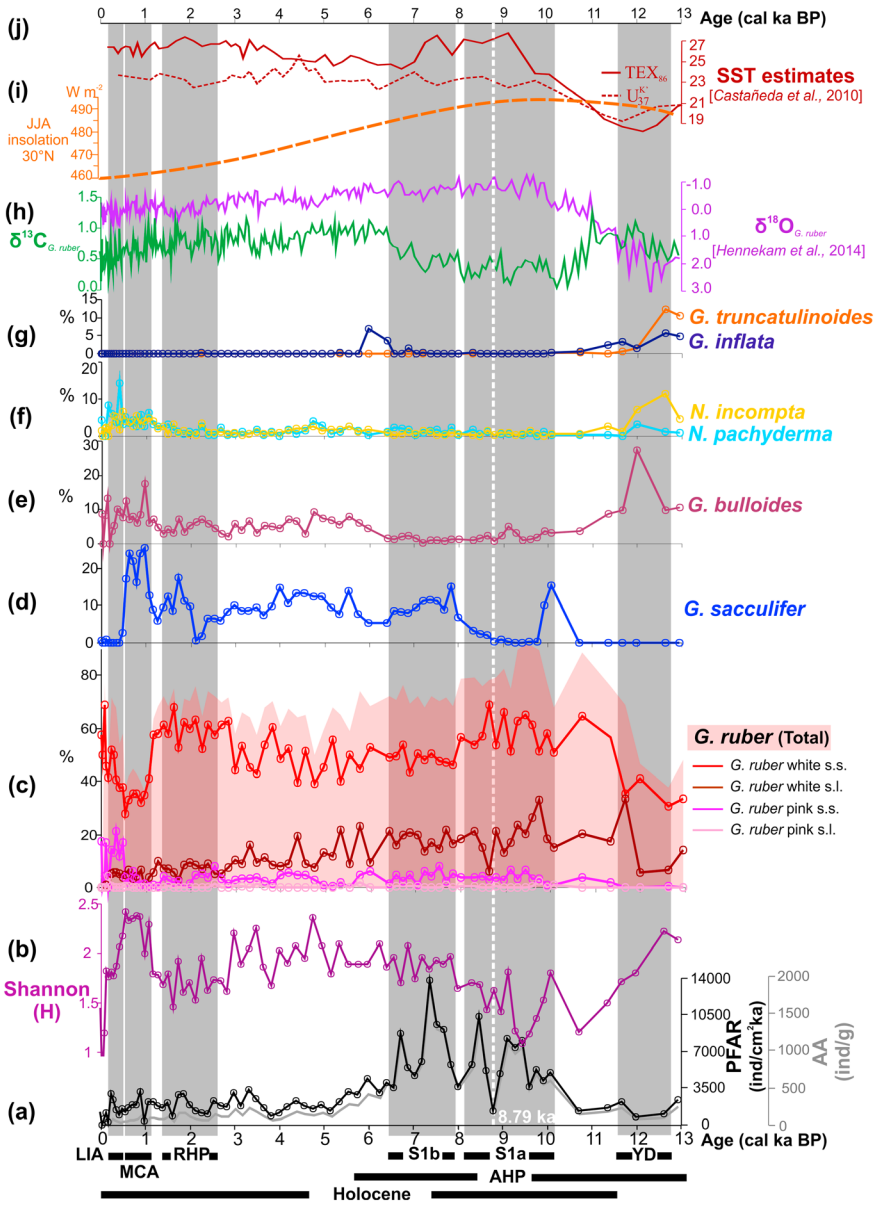

Figure 2. (a) Total planktic accumulation rate (PFAR) and total absolute abundances (AA). (b) Diversity index (Shannon *H*). (c–g) Relative abundances (%) of the most representative planktic foraminifer species. (h) Oxygen and carbon stable isotopes. (i) Summer insolation curve at 30°N [*Laskar et al.*, 2004]. (j) TEX_{86} and $U^{k'}_{37}$ SST estimates (GeoB 7702-3; Figure 1). The main short-term events are indicated in light grey (YD: Younger Dryas; S1a and S1b: the two phases of sapropel 1 as defined by *Hennekam et al.* [2014] in the sediment from the same core (PS009PC); RHP: Roman Humid Period; MCA: Medieval Climatic Anomaly; LIA: Little Ice Age). The main climatic phases are also reported: Holocene and African Humid Period (AHP).

at 8.8 ka, followed by a progressive decrease to small average sizes of ~200 μm and ~280 μm around 5.5 ka. Test size changes over the past ~5.5 ka were much less strong than those before 5.5 ka. Overall, *G. ruber* s.l. was characterized by more size variability than *G. ruber* s.s. This larger size variability likely results from our classification scheme rather than from ecological cause, with *G. ruber* s.l. encompassing all morphotypes other than *G. ruber* s.s. and hence a wider range in test size (Plate 1). A general long-term increase in size of *O. universa* occurred until ~3.0 ka (Figure 3c). From 3.0 ka to the top of core, the general size increase of *O. universa* included two intervals of significant size minima at 1.7 ka (434 ± 63 μm) and 0.5 ka (497 ± 38 μm) (Figure 3c and Table 2).

Table 1. Raw Data of Foraminifer Counts After Extrapolation Using the Different Splits

						Globigerinoides								*Orbulina*		*Neogloboquadrina*		
Midpoint Sediment Depth (cm)	Age (cal ka B.P.)	Sedimentation Rate (cm/Ka)	Wet Weight (g)	Dry Weight (g)	Split	*G. ruber alba s.s.*	*G. ruber alba s.l.*	*G. ruber rosea s.s.*	*G. ruber rosea s.l.*	*G. conglobatus*	*G. sacculifer sac*	*G. quadrilobatus*	*G. trilobus*	*O. universa*	*O. universa juvénile*	*N. pachyderma s.*	*N. incompta*	*N. dutertrei*
1.5	−0.012	114.1	16.2	6.6	1	80	0	24	0	0	1	0	0	2	0	6	2	0
5.5	0.026	106.0	13.5	5.4	1	2	0	0	0	0	0	0	0	2	0	0	0	0
9.5	0.068	96.0	9.6	3.9	1	33	2	2	0	0	0	0	0	3	0	0	1	0
13.5	0.113	87.8	11.9	4.9	1	59	1	22	0	0	0	0	1	7	0	3	3	0
17.5	0.163	80.9	9.0	3.8	1	10	0	0	1	2	0	0	0	5	0	2	0	0
21.5	0.216	74.9	10.6	4.4	1	178	17	49	2	5	0	0	0	11	0	21	10	2
25.5	0.273	69.8	7.9	3.3	1	114	13	30	0	3	0	0	0	15	0	12	12	0
29.5	0.334	65.4	7.7	3.2	1	57	8	30	0	2	0	0	0	5	0	5	7	0
33.5	0.400	61.4	8.8	3.8	1	45	6	14	0	1	0	0	0	5	0	17	2	0
37.5	0.469	58.0	9.7	4.4	1	87	9	39	0	3	0	2	4	18	0	7	15	0
41.5	0.541	54.9	8.9	3.9	1	49	8	7	1	0	4	9	17	17	1	9	7	0
45.5	0.618	52.1	9.8	4.2	1	86	17	5	1	0	16	15	32	22	2	9	10	0
49.5	0.699	49.5	10.2	4.4	1	116	11	20	0	1	12	22	38	15	0	14	8	0
53.5	0.784	47.3	7.7	3.4	1	92	11	8	0	3	12	6	24	16	0	7	14	0
57.5	0.872	45.2	9.0	3.7	1	156	33	5	0	4	35	21	62	24	0	28	14	0
61.5	0.965	43.3	9.7	4.2	1	26	0	1	0	2	6	2	11	5	0	2	3	0
65.5	1.061	41.5	10.5	4.5	1	184	18	2	0	3	9	17	32	27	2	28	22	0
69.5	1.161	39.9	10.6	4.5	1	272	26	4	0	4	3	9	30	13	3	15	19	0
73.5	1.265	38.4	9.1	4.0	1	203	34	2	0	5	3	6	12	5	2	9	7	1
77.6	1.376	37.0	11.2	4.7	1	240	27	16	0	3	13	8	16	4	0	10	10	0
81.6	1.488	35.7	10.3	4.4	1	286	35	14	2	3	19	31	12	3	0	15	3	0
85.6	1.604	34.5	11.3	4.9	1	149	12	4	0	0	6	9	4	1	0	4	7	1
89.6	1.724	33.4	9.2	4.2	1/2	351	20	16	0	6	30	28	58	16	10	8	6	0
93.6	1.848	32.3	9.8	4.3	1/2	463	64	0	0	14	22	22	40	16	4	4	10	0
97.6	1.976	31.3	10.4	4.4	1	294	46	6	0	7	7	17	24	5	1	6	3	1
101.6	2.108	30.4	10.6	4.4	1	227	30	17	0	7	0	0	2	16	0	3	1	0
105.6	2.243	29.5	10.4	4.4	1	159	22	16	0	3	0	1	4	10	0	8	10	0
109.6	2.382	28.7	10.0	4.2	1	166	24	10	0	3	3	5	10	5	0	1	2	0
113.6	2.526	27.9	10.5	4.6	1/2	391	36	56	10	8	2	10	32	2	0	2	6	0
117.6	2.673	27.2	11.9	5.4	1/2	393	32	22	0	4	8	10	20	28	0	14	8	0
121.6	2.824	26.5	10.7	4.9	1/2	359	42	8	0	6	8	12	28	14	0	2	4	0
125.6	2.979	25.8	9.6	4.2	1/2	391	92	26	4	14	16	22	52	22	0	6	8	0
129.6	3.138	25.2	10.3	4.7	1/2	313	52	20	2	4	4	14	32	8	2	6	2	0
133.6	3.301	24.6	9.5	4.3	1/2	453	162	32	0	8	10	26	50	22	0	6	6	0
137.6	3.468	24.0	8.4	3.8	1/2	285	62	26	8	8	17	14	32	20	0	12	8	0
141.6	3.639	23.4	8.9	3.9	1	253	53	11	2	4	3	10	22	7	1	1	3	0
145.6	3.813	22.9	10.6	4.5	1	168	24	4	0	2	5	7	15	6	0	3	2	0
149.6	3.992	22.4	8.3	3.6	1	154	25	15	0	6	18	5	24	1	0	0	3	0
153.6	4.174	21.9	10.5	4.8	1/2	345	60	38	0	12	19	20	32	2	0	12	10	0
157.6	4.361	21.5	9.8	4.4	1/2	327	160	40	0	2	26	16	68	4	0	4	16	0
161.6	4.551	21.0	9.3	4.1	1/2	321	56	28	0	4	19	12	52	10	2	8	12	0
165.6	4.745	20.6	7.9	3.4	1	177	33	13	1	5	21	4	31	13	2	18	12	0
169.6	4.943	20.2	10.1	4.6	1/2	343	100	6	0	6	31	24	38	18	0	22	10	4
173.6	5.145	19.8	12.0	5.3	1/2	343	72	2	0	8	19	6	34	6	6	4	10	0
177.2	5.330	19.4	9.5	4.2	1/2	341	186	18	10	8	20	4	42	22	2	10	14	0
181.2	5.540	19.1	9.6	4.2	1/4	597	108	0	0	12	24	20	124	28	0	32	32	0
185.2	5.753	18.8	11.0	5.0	1/4	609	312	64	24	4	15	24	68	4	12	20	16	0
189.2	5.970	18.4	10.2	4.5	1/4	1001	176	116	0	16	35	12	56	24	0	4	32	0
193.2	6.240	14.8	11.7	5.3	1/4	686	460	41	52	12	46	16	68	4	0	24	32	0
195.2	6.399	12.5	7.9	3.5	1/4	979	424	32	4	0	37	20	52	56	0	24	16	0
197.2	6.559	12.5	13.3	6.1	1/8	1501	488	144	8	24	57	48	152	56	16	72	8	0
199.2	6.719	12.5	8.6	4.0	1/16	2551	944	112	16	0	89	144	160	80	0	96	32	0
201.2	6.878	12.5	8.4	3.8	1/8	1245	592	136	16	8	49	48	136	56	0	48	32	0
203.2	7.038	12.5	12.2	5.3	1/8	1711	672	32	16	0	129	88	104	56	0	8	16	0
205.2	7.197	12.5	11.5	5.0	1/8	2013	576	248	0	8	137	184	152	80	0	32	64	0
207.2	7.357	12.5	8.5	3.7	1/16	3495	1184	288	16	16	249	320	240	112	0	96	80	0
209.2	7.516	12.5	9.8	4.3	1/16	2677	816	448	0	0	137	176	320	112	16	96	16	0
211.2	7.676	12.5	11.4	5.1	1/16	2967	1360	144	48	0	185	224	160	256	0	32	16	0

Table 1. Raw Data of Foraminifer Counts After Extrapolation Using the Different Splits

	Globoturborotalia				*Globorotalia*		*Beela*		*Globigerinella*		*Globigerinita*								
Globigerina bulloides	*G. rubescens white*	*G. rubescens pink*	*G. tenella*	*G. inflata*	*G. crassaformis*	*G. truncatulinoides*	*B. digitata*	*B. megastoma*	*G. siphonifera I*	*G. siphonifera II*	*G. calida*	*G. glutinata*	*G. uvula*	*G. minuta*	*Hastigerina pelagica*	*Tenuitella parkerae*	*Dentagloborotalia anfracta*	Undetermined	TOTAL
12	2	0	0	0	0	0	0	0	0	2	1	1	0	0	0	0	0	6	139
0	0	0	0	0	0	0	0	0	0	0	0	0	0	0	0	0	0	0	4
4	0	0	1	0	0	0	0	0	0	0	0	0	0	0	0	0	0	2	48
17	2	1	2	0	0	0	0	0	0	1	4	4	0	0	0	0	0	2	129
0	0	0	1	0	0	0	0	0	0	1	0	1	0	0	0	0	0	1	24
13	8	1	10	0	0	0	0	0	1	3	5	3	0	0	0	0	0	3	342
12	0	0	2	0	0	0	0	0	0	2	2	1	0	0	1	0	0	8	227
14	3	0	5	0	0	0	0	0	0	0	0	1	0	0	1	0	0	2	140
11	5	0	2	0	0	0	0	1	0	3	1	1	0	0	0	0	0	6	120
18	7	3	2	0	0	0	0	4	0	2	3	3	0	0	1	0	0	5	232
22	6	6	5	0	0	0	0	0	0	0	4	0	0	0	2	0	0	1	175
19	6	3	4	0	0	0	0	0	0	1	6	3	0	0	0	0	0	4	261
26	5	5	10	0	0	0	0	5	1	4	5	3	0	0	2	0	0	4	327
16	12	1	13	0	0	0	0	4	0	3	0	7	0	0	2	0	0	8	259
41	6	0	20	0	0	0	1	7	0	1	7	4	0	0	9	0	0	11	489
13	1	0	0	0	0	0	0	0	0	0	1	1	0	0	0	0	0	0	74
28	9	3	15	0	0	0	6	10	0	6	6	0	0	0	12	0	0	10	449
34	7	3	3	0	0	0	2	12	0	3	2	5	0	0	3	0	0	1	473
17	1	0	10	0	0	0	3	10	0	4	2	9	0	0	1	0	0	3	349
11	3	0	7	0	0	0	4	10	0	0	2	4	0	0	1	0	0	3	392
21	2	0	8	0	0	0	2	5	6	9	1	6	0	0	4	0	0	6	493
7	0	0	4	0	0	0	0	1	5	2	1	1	0	0	2	0	0	0	220
48	6	0	10	0	0	0	0	4	8	26	0	6	0	0	4	0	0	4	665
26	6	0	6	0	0	0	0	12	6	14	0	2	0	0	4	0	0	6	741
26	2	1	7	0	0	0	0	8	6	10	0	10	0	0	0	0	0	5	492
23	4	0	4	0	0	0	0	6	4	5	0	5	0	0	2	0	0	4	360
22	5	1	12	1	0	0	0	3	4	5	1	11	0	0	2	0	0	4	304
16	4	2	2	0	0	0	0	3	7	2	0	1	0	0	0	0	0	4	270
30	6	0	18	0	0	0	0	2	12	36	0	4	0	0	0	0	0	18	681
18	16	6	4	0	0	0	0	10	14	18	0	6	0	0	4	0	0	4	639
12	16	0	10	0	0	0	0	0	18	16	2	6	0	0	0	0	0	8	571
52	12	12	44	0	0	0	8	16	18	34	4	14	0	0	2	0	0	12	881
24	20	4	16	0	0	0	0	4	6	32	0	4	0	0	0	0	0	16	585
66	22	12	24	0	0	0	0	6	22	28	0	32	0	0	4	0	0	14	1005
22	16	6	52	0	0	0	0	14	4	22	4	16	0	0	0	0	0	16	664
25	9	6	26	0	0	0	0	2	4	8	2	11	0	0	0	0	0	7	470
14	7	0	5	0	0	0	0	4	4	2	0	3	0	0	0	0	0	3	278
14	10	8	10	0	0	0	0	2	4	7	0	2	0	0	2	0	0	8	318
48	6	4	10	0	0	0	0	6	12	0	2	8	0	0	4	0	0	8	658
54	18	16	14	0	0	0	0	14	12	10	0	14	0	0	2	0	0	6	823
18	2	2	20	0	0	0	0	6	20	12	6	6	0	0	0	0	0	6	622
42	14	10	10	0	0	0	1	6	6	9	5	5	0	0	4	0	0	8	450
56	6	8	14	0	0	0	0	2	4	32	0	18	0	2	4	0	0	6	754
42	8	6	10	0	0	0	0	8	6	12	2	4	0	0	0	0	0	8	616
48	22	2	22	2	0	0	6	0	2	26	4	32	0	0	2	0	0	6	851
96	32	4	0	0	0	0	0	0	12	8	4	36	0	0	8	0	0	16	1193
84	0	12	16	0	0	0	4	0	16	24	4	8	0	0	4	0	0	16	1360
84	24	8	16	128	0	0	0	16	12	76	8	20	0	0	4	0	0	20	1888
60	28	4	32	196	0	0	8	12	8	52	0	16	0	0	4	0	0	32	1893
32	28	8	20	72	0	0	8	8	8	68	40	48	0	0	4	0	0	8	1996
40	32	40	40	0	0	0	16	16	40	80	24	96	0	0	0	0	0	32	3030
96	64	48	48	0	0	0	0	0	48	80	48	64	0	0	0	0	0	16	4736
72	32	16	16	40	0	0	8	24	64	80	56	56	0	8	8	0	0	24	2870
56	0	0	16	0	0	0	0	0	16	72	128	208	0	0	16	8	0	24	3376
16	8	8	8	8	0	0	32	8	72	96	104	240	0	0	0	0	0	72	4166
80	32	0	48	0	0	0	16	32	32	96	176	256	0	0	0	0	0	32	6896
64	16	0	128	0	0	0	32	0	64	176	80	224	0	0	0	0	0	16	5614
48	48	16	80	0	0	0	32	16	96	112	48	336	0	0	16	32	0	48	6320

Table 1. Continued

						Globigerinoides								*Orbulina*		*Neogloboquadrina*		
Midpoint Sediment Depth (cm)	Age (cal ka B.P.)	Sedimentation Rate (cm/Ka)	Wet Weight (g)	Dry Weight (g)	Split	*G. ruber alba s.s.*	*G. ruber alba s.l.*	*G. ruber rosea s.s.*	*G. ruber rosea s.l.*	*G. conglobatus*	*G. sacculifer sac*	*G. quadrilobatus*	*G. trilobus*	*O. universa*	*O. universa juvénile*	*N. pachyderma s.*	*N. incompta*	*N. dutertrei*
213.2	7.836	12.5	11.6	5.1	1/8	1839	664	209	8	16	113	192	296	48	0	96	32	8
215.2	7.995	12.5	9.9	4.6	1/8	1272	416	81	8	0	36	16	40	56	0	8	16	0
219.2	8.314	12.5	10.8	4.9	1/8	2023	800	136	24	0	57	32	32	112	0	64	16	0
221.2	8.474	12.5	10.8	4.9	1/16	3825	1008	288	0	16	56	48	48	192	48	32	0	0
223.2	8.634	12.5	11.9	5.4	1/8	2573	232	112	0	0	15	24	40	120	0	40	48	0
225.2	8.793	12.5	9.6	4.3	1/2	421	164	30	4	4	1	2	0	38	6	2	2	0
227.2	8.953	12.5	12.2	5.4	1/8	2317	464	104	0	0	2	8	24	64	0	24	32	8
229.2	9.112	12.5	11.4	5.0	1/16	2805	912	368	0	16	2	0	16	144	80	32	48	0
231.2	9.272	12.5	10.5	4.8	1/16	2903	1088	160	0	0	0	0	0	64	0	16	16	0
233.2	9.431	12.5	13.1	5.9	1/16	4069	1280	416	0	0	0	0	0	304	16	16	32	0
235.2	9.591	12.5	12.5	5.9	1/8	1711	736	88	8	8	0	8	0	24	0	24	40	8
237.2	9.751	12.5	11.1	5.3	1/8	1853	1192	120	80	16	0	8	0	56	0	0	16	0
239.2	9.910	12.5	10.7	5.0	1/8	1575	496	32	0	0	73	128	72	40	0	32	0	0
241.2	10.070	12.5	9.7	5.0	1/8	1493	448	32	32	8	225	160	72	0	0	8	16	0
249.2	10.708	12.5	11.6	6.0	1/2	564	176	34	0	2	0	0	0	0	0	2	6	0
257.2	11.346	12.5	10.7	5.9	1/2	581	180	18	0	2	0	0	0	0	0	4	26	0
261.2	11.666	12.5	11.9	6.5	1/4	541	508	0	0	20	0	0	0	0	0	0	16	0
265.2	11.985	12.5	10.9	5.7	1	187	26	0	0	1	0	0	0	0	0	15	33	0
273.2	12.623	12.5	12.1	6.5	1/2	213	46	2	0	0	0	0	0	0	2	8	80	0
277.2	12.942	12.5	11.8	6.3	1/4	517	220	0	0	4	0	0	0	12	4	12	72	0

5. Discussion

The most prominent feature observed in the planktic foraminifer variability is the pronounced deviation during the 10 to 6 ka time interval. This is not only expressed in foraminifer diversity and total foraminifer test fluxes (PFAR; Figure 2) but also in test morphology (Figure 3). This time period corresponds largely with the African Humid Period and with the time period of sapropel S1 deposition. Excessive Nile outflow ("deluge") has been postulated for this period [e.g., *Rossignol-Strick et al*., 1982]. The surface water ecology as represented by the foraminifer assemblages in our core, which is under the influence of the Nile outflow, is thus likely to reflect at least partly the variability in Nile outflow (Figures 4a and 4b).

5.1. Effect of Nile River Discharge on the Planktic Foraminifer Community During the Holocene in the Southeastern Levantine Basin

The tropical-subtropical species *Globigerinoides ruber* was dominant throughout our paleo- record. In the modern Mediterranean Sea, *G. ruber* proliferates mainly in summer in nutrient-depleted warm surface (0–50 m) waters [*Pujol and Vergnaud-Grazzini*, 1995; *Reiss et al*., 1999]. In addition, *G. ruber* is possibly the most euryhaline tropical-subtropical planktic foraminifer species [*Ufkes et al*., 1998; *Schmuker and Schiebel*, 2002; *Rohling et al*., 2004].

Along our record, *G. ruber* white was largely dominant over *G. ruber* pink. *Principato et al*. [2003, 2006] find also a dominance of *G. ruber* white west southwest of Crete (Figure 1) during the Holocene. In contrast, *Pujol and Vergnaud-Grazzini* [1995] (Figure 1) show that the modern assemblages of the Levantine Basin southwest of Cyprus are dominated by *G. ruber* pink, although they emphasize the dominance of *G. ruber* white to the east of 18°E. These discrepancies are possibly linked to regional differences in physical-chemical properties of surface water masses controlled by the hydrology of the basin. In fact, our site is under the direct influence of Nile River discharge (Figure 1). Therefore, surface water salinities, turbidity and nutrient availability may vary at the regional scale. At our core location, surface waters are more productive than the oligotrophic waters off Cyprus [e.g., *Schmiedl et al*., 2003]. Unlike *G. ruber* pink, *G. ruber* white proliferates also during winter [*Pujol and Vergnaud-Grazzini*, 1995], which might explain its advantage over the former in this environment. Moreover, since the Aswan High Dam was finished in the 1960s, the effect of the Nile has largely diminished. Before the Aswan High Dam, the Nile runoff was more important for the surface water

Table 1. Continued

	Globoturborotalia				Globorotalia		Beela		Globigerinella		Globigerinita								
Globigerina bulloides	*G. rubescens white*	*G. rubescens pink*	*G. tenella*	*G. inflata*	*G. crassaformis*	*G. truncatulinoides*	*B. digitata*	*B. megastoma*	*G. siphonifera I*	*G. siphonifera II*	*G. calida*	*G. glutinata*	*G. uvula*	*G. minuta*	*Hastigerina pelagica*	*Tenuitella parkerae*	*Dentagloborotalia anfracta*	Undetermined	TOTAL
56	64	24	8	0	0	0	40	8	64	56	0	112	0	0	8	0	0	16	3977
32	48	16	8	0	0	0	0	0	8	48	56	56	0	0	0	16	0	16	2253
40	32	32	24	8	0	0	24	16	24	112	24	88	0	0	24	0	0	24	3768
112	112	208	32	0	0	0	0	0	224	80	80	240	0	0	0	0	0	80	6729
88	32	48	8	0	0	0	8	32	32	112	16	104	0	0	8	0	0	40	3732
6	10	0	2	0	0	0	18	0	18	12	4	24	0	0	10	0	0	2	780
88	56	40	56	0	0	0	40	8	32	56	0	64	0	0	8	0	0	8	3503
272	64	32	80	0	0	0	112	32	96	144	16	64	0	0	48	0	0	48	5431
144	48	0	32	0	0	0	16	0	16	32	0	0	0	0	48	32	0	16	4631
64	32	0	0	0	0	0	0	0	16	16	0	0	0	0	0	0	0	0	6261
40	56	24	0	0	0	0	0	0	8	0	0	0	0	0	0	0	0	8	2791
64	64	0	8	0	0	0	0	32	80	24	0	0	0	0	0	0	0	0	3613
104	40	0	0	0	0	0	0	0	32	24	8	56	0	0	0	0	0	8	2720
96	40	0	32	8	16	8	0	0	8	104	0	128	0	0	0	0	0	8	2942
32	16	4	6	6	0	2	0	0	0	0	0	18	0	0	0	0	0	6	874
90	10	0	48	26	0	0	0	0	0	0	0	22	0	0	0	8	6	6	1027
148	44	4	16	52	52	8	0	0	0	0	0	24	0	0	0	0	0	88	1521
125	10	2	4	7	0	7	0	0	0	0	1	18	0	0	0	8	6	7	457
68	60	20	10	40	4	86	0	0	0	0	0	26	0	0	0	8	4	16	693
164	88	32	60	72	0	160	0	0	0	0	0	84	0	0	0	12	0	20	1533

ecology as it is today. This might also be responsible for the differences observed between our fossil pre-Aswan fauna and the modern post-Aswan Levantine assemblages [*Pujol and Vergnaud-Grazzini*, 1995].

The two morphotypes of *G. ruber* white s.s. and s.l. might indicate a variability in Nile River discharge over time. The two *G. ruber* morphotypes occupy slightly different depth habitats in the upper water column, with *G. ruber* s.s. living in the upper ~30 m and *G. ruber* s.l. living on average below at 30–50 m depth [*Wang*, 2000]. Since its presence requires a deep penetration of nutrients in the water column as observed in the southern China Sea by *Wang* [2000], high proportions of *G. ruber* s.l. indicate enhanced nutrient input and surface water productivity. High proportions of *G. ruber* s.l. were found in our early record and during sapropel S1 supporting the hypothesis of enhanced primary production at that time interval.

Very high PFAR values, mainly caused by *G. ruber*, were recorded during S1 and starting to increase slightly before its deposition (Figure 2a). For instance, those PFAR values were of the same order of magnitude as those found presently in the productive waters off the French Atlantic coast at the same water depth [e.g., *Mojtahid et al*., 2013]. Although *G. ruber* is known to generally inhabit oligotrophic waters, its increase in absolute abundance during sapropel S1 testifies the perseverance of this species in low-saline surface waters, while other species are more disadvantaged. This also explains its continuous dominance along the record regardless of the significant changes in surface water characteristics. High PFAR values constitute another proof on enhanced primary production during S1. *Rohling and Gieskes* [1989] and *Incarbona et al*. [2011] emphasize the presence of a deep chlorophyll maximum to explain peaks of *Neogloboquadrina pachyderma* dextral (=*N. incompta*) and lower photic zone coccolithophore species in some sapropels. However, more pronounced stratification due to increased Nile discharge was likely also very important for the onset of S1 in the eastern Mediterranean as indicated by the decline in deep-dwelling foraminifer species (e.g., *Globorotalia truncatulinoides* and *Globorotalia inflata*; Figure 2g). Indeed, a drop of about 2.0 to 4.0 units in the eastern Mediterranean sea surface salinity during S1 compared to the present values was reported [e.g., *Kallel et al*., 1997; *Myers et al*., 1998]. Because our core was retrieved from a marginal environment with a strong regional context (influence of Nile River discharge), sea surface salinities and temperatures can neither be accurately reconstructed from $\delta^{18}O_{G.\ ruber}$ [*Hennekam et al*., 2014] nor from transfer functions based on modern planktic foraminifer assemblages. In our case, the transition to most depleted $\delta^{18}O_{G.\ ruber}$ values during the start of S1 (Figure 2h) indicated the highest Nile discharge of the Holocene [*Hennekam et al*., 2014] and is confirmed by Ba/Ca data on *G. ruber* from the same area [*Weldeab et al*., 2014]. The near-simultaneous increase in Nile

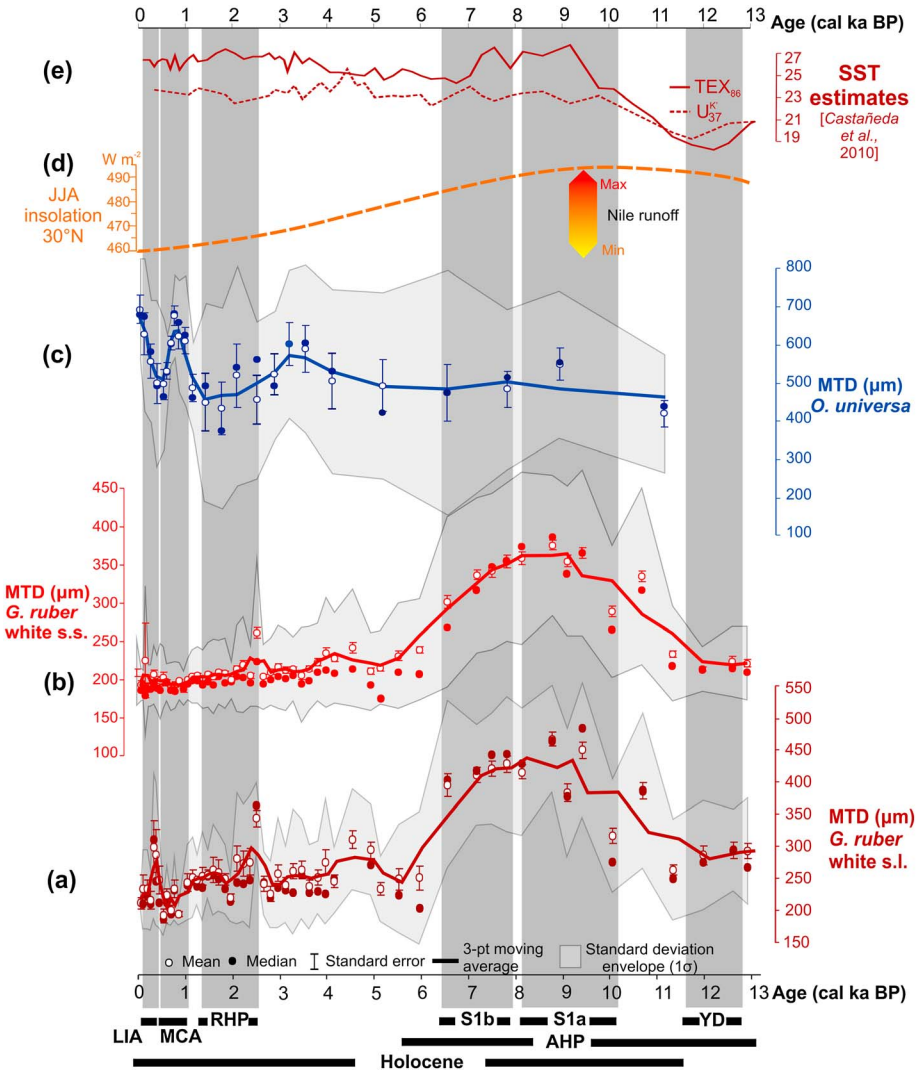

Figure 3. (a) Minimum test diameters (MTD in µm) of *G. ruber* white s.s.; (b) MTD (in µm) of *G. ruber* white s.l.; (c) MTD (in µm) of *O. universa* after summing up some samples to obtain at least 10 individuals; see Table 2 for details; (d) summer insolation curve at 30°N [*Laskar et al.*, 2004]; (e) TEX_{86} and $U^{k'}_{37}$ SST estimates (GeoB 7702-3; Figure 1) are plotted. The main events and climatic phases are reported similar to Figure 1.

discharge and trace element enrichment (*V*/Al, proxy for low oxygen conditions) [*Hennekam et al.*, 2014] indicates that a more sluggish ventilation due to buoyancy gain by Nile fresh water is probable. Nevertheless, planktic foraminifer characteristics show that enhanced productivity would have contributed to the low oxygen conditions during S1.

5.2. Control of Nile River Discharge on the Size of Planktic Foraminifers

Planktic foraminifer test size can be indicative of surface water ecology. However, the environmental factors controlling foraminifer size are still poorly understood. Optimum environmental conditions, i.e., temperature, salinity, nutrition, oxygen, and others, may affect growth rates and size of planktic foraminifer tests [e.g., *Hecht*, 1976; *Schmidt et al.*, 2004a].

For instance, planktic foraminifer metabolism is known to accelerate with temperature and approximately doubles when temperature increases by 10°C [e.g., *Bijma et al.*, 1990; *Spero et al.*, 1991]. In our record, test size of *Globigerinoides ruber* (white) was significantly larger during sapropel S1 than before and after S1 (Figures 3 and 4), and high sea surface temperatures (SSTs) were reconstructed for S1 (Figure 2j) [*Castañeda et al.*, 2010]. Although positive correlation between temperature and test size has previously been observed

Paleoceanography

10.1002/2014PA002705

Table 2. Minimum Test Diameters (MTD in μm) Data and the Number of Measured Specimens of *G. ruber* White s.s. and s.l. and *O. universa*

		G. ruber white s.s.					*G. ruber* white s.l.					*O. universa*							
												All Samples		Average Values for Summed Up Samples to Obtain >10 Individuals					
Age (cal ka B.P.)	Depth (cm)	Mean (μm)	Median (μm)	Standard Deviation (1σ Error) (μm)	No. of Specimens	Standard Error (μm)	Mean (μm)	Median (μm)	Standard Deviation (1σ error) (μm)	No. of Specimens	Standard Error (μm)	Mean (μm)	No. of Specimens	Mean Age (cal ka B.P.)	Mean MTD (μm)	Median (μm)	Standard Deviation (1σ Error) (μm)	No. of Specimens	Standard Error (μm)
−0.012	1.5	208.7	202.0	42.3	67	5.1						845.7	1						
0.026	5.5											695.1	2						
0.068	9.5	193.3	186.1	21.8	24	4.4	210.8	210.8	12.3	2	8.7	684.4	3						
0.113	13.5	193.0	193.4	19.0	42	2.9	232.8	209.5	62.6	8	22.1	555.1	7	0.049	695.1	681.4	133.3	13	37.0
0.163	17.5	232.7	178.7	97.9	4	44.0						664.0	2						
0.216	21.5	192.0	187.0	26.9	152	2.2	232.6	220.0	62.2	17	15.1	595.3	11	0.189	629.7	675.4	199.1	13	55.2
0.273	25.5	192.3	187.8	26.8	84	2.9	214.7	209.5	48.2	12	13.9	558.8	13	0.273	558.8	583.3	160.8	13	44.6
0.334	29.5	206.5	194.6	38.7	36	6.4	299.3	309.8	113.2	8	40.0	407.4	3						
0.400	33.5	195.5	189.4	36.0	34	6.1	287.1	245.8	112.0	8	39.6	502.3	4						
0.469	37.5	197.7	185.7	49.6	60	6.4	246.7	211.7	75.1	11	22.6	591.0	10	0.401	500.2	494.4	219.4	17	53.2
0.541	41.5	202.8	197.4	40.3	37	6.6	190.6	186.0	30.3	8	10.7	497.9	19	0.541	497.9	465.6	171.9	19	39.4
0.618	45.5	196.7	196.3	24.2	59	3.1	222.3	210.9	45.8	16	11.5	533.1	19	0.618	533.1	529.8	97.1	19	22.3
0.699	49.5	191.0	186.6	31.5	92	3.3	199.7	193.4	24.0	10	7.6	606.8	11	0.699	606.8	605.3	60.0	11	18.1
0.784	53.5	193.8	184.3	30.5	69	3.6	232.9	231.5	49.3	11	14.9	677.5	17	0.784	677.5	683.0	109.0	17	26.4
0.872	57.5	198.4	195.3	24.2	136	2.1	192.6	192.8	18.1	20	4.0	624.7	18	0.872	624.7	660.4	147.3	18	34.7
0.965	61.5	187.4	188.1	22.2	12	5.8						671.4	5						
1.061	65.5	200.6	194.2	26.9	157	2.1	242.9	239.4	59.9	17	14.5	554.0	19	1.013	612.7	626.9	171.8	24	35.1
1.161	69.5	204.4	197.9	34.9	248	2.2	250.6	244.6	64.2	26	12.6	489.1	11	1.161	489.1	462.0	119.4	11	36.0
1.265	73.5	205.9	198.3	36.5	174	2.8	246.7	236.7	39.8	34	6.8	557.1	5						
1.376	77.6	200.7	193.6	37.7	207	2.6	252.1	235.4	69.5	26	13.6	544.9	3						
1.488	81.6	206.1	197.0	42.9	261	2.6	255.5	253.2	38.5	35	6.5	506.3	3						
1.604	85.6	204.3	193.3	48.8	121	4.4	262.7	253.9	71.0	12	20.5	195.1	1	1.434	450.9	494.2	260.5	12	75.2
1.724	89.6	209.6	204.6	41.6	154	3.3	258.3	248.0	61.6	10	19.5	390.6	8						
1.848	93.6	208.1	195.1	45.6	215	3.1	248.1	232.3	54.6	33	9.5	478.5	7	1.786	434.6	375.1	264.8	15	68.4
1.976	97.6	199.8	197.6	24.4	241	1.6	219.0	213.8	36.7	42	5.7	443.1	4						
2.108	101.6	214.5	204.3	56.6	197	4.0	280.6	243.5	103.8	28	19.6	528.1	1						
2.243	105.6	219.7	202.1	62.9	130	5.5	273.4	241.5	92.7	22	19.8	591.2	7	2.109	520.8	542.7	289.0	12	83.4
2.382	109.6	205.4	195.9	39.7	134	3.4	275.5	246.8	104.0	25	20.8	564.0	2						
2.526	113.6	261.2	223.2	95.8	183	7.1	343.5	364.1	56.7	21	12.4	172.5	1						
2.673	117.6	203.9	194.2	42.5	171	3.2	240.8	241.9	50.1	16	12.5	633.3	8	2.527	456.6	564.0	206.8	11	62.4
2.824	121.6	210.3	200.2	43.6	145	3.6	224.5	218.8	52.2	19	12.0	647.3	1						
2.979	125.6	216.3	204.7	53.8	182	4.0	257.6	235.9	86.9	46	12.8	399.7	9	2.902	523.5	493.7	169.3	10	53.5
3.138	129.6	212.8	201.0	52.9	138	4.5	239.2	230.4	60.4	26	11.8	639.9	4						
3.301	133.6	213.8	205.1	41.1	203	2.9	260.6	227.4	98.2	77	11.2	569.4	8	3.220	604.7	604.4	195.0	12	56.3
3.468	137.6	206.0	194.9	61.6	125	5.5	263.4	254.7	78.0	32	13.8	659.1	8						
3.639	141.6	214.3	199.0	54.6	213	3.7	236.6	227.8	66.3	51	9.3	524.5	5	3.553	591.8	606.3	221.0	13	61.3
3.813	145.6	223.0	209.2	50.2	125	4.5	250.8	229.1	56.6	24	11.6	521.0	4						
3.992	149.6	235.5	212.4	70.9	112	6.7	274.9	224.4	98.0	24	20.0	518.7	1						
4.174	153.6	228.5	207.9	59.2	146	4.9	245.0	248.3	52.6	27	10.1	464.9	1						
4.551	161.6	239.9	214.2	76.3	125	6.6	310.1	309.7	79.0	29	14.7	519.6	5	4.133	506.0	533.2	241.9	11	72.9
4.943	169.6	210.6	193.4	51.0	158	4.1	293.6	270.9	71.6	32	12.7	656.8	7						
5.145	173.6	215.6	173.9	47.9	149	3.9	232.9	225.2	50.7	26	9.9	422.9	2						
5.540	181.2	231.4	209.8	69.0	131	6.0	248.7	224.0	86.0	26	16.9	402.5	4	5.209	494.1	422.9	245.5	13	68.1
5.970	189.2	239.2	208.1	66.0	216	4.5	250.3	202.5	103.8	30	18.9	420.0	4						
6.559	197.2	301.9	268.4	110.7	168	8.5	396.1	402.9	131.9	55	17.8	521.0	5						
7.197	205.2	336.4	318.0	101.0	255	6.3	411.8	420.2	78.8	47	11.5	488.5	10	6.575	476.5	479.3	322.3	19	73.9

Table 2. (continued)

		G. ruber white s.s.					*G. ruber* white s.l.					*O. universa*							
												All Samples		Average Values for Summed Up Samples to Obtain >10 Individuals					
Age (cal ka B.P.)	Depth (cm)	Mean (µm)	Median (µm)	Standard Deviation (1σ Error) (µm)	No. of Specimens	Standard Error (µm)	Mean (µm)	Median (µm)	Standard Deviation (1σ error) (µm)	No. of Specimens	Standard Error (µm)	Mean (µm)	No. of Specimens	Mean Age (cal ka B.P.)	Mean MTD (µm)	Median (µm)	Standard Deviation (1σ Error) (µm)	No. of Specimens	Standard Error (µm)
7.516	209.2	341.8	347.4	102.0	182	7.5	421.5	443.0	86.7	51	12.1	548.3	7						
7.836	213.2	354.0	355.9	103.4	155	8.3	428.7	442.4	106.4	69	12.8	378.5	5						
8.155	217.2	358.7	373.1	112.7	193	8.1	416.4	428.8	101.0	76	11.6	530.6	8	7.836	485.8	513.8	211.1	20	47.2
8.793	225.2	375.6	386.0	91.5	199	6.5	467.7	467.2	83.9	56	11.2	598.1	15						
9.112	229.2	354.8	339.4	98.0	155	7.9	383.7	378.8	102.0	53	14.0	502.6	6	8.953	550.4	553.8	194.4	21	42.4
9.431	233.2	365.3	365.0	108.5	231	7.1	450.2	483.9	105.7	68	12.8	498.7	19						
10.070	241.2	289.2	265.3	85.9	153	6.9	315.8	275.9	89.0	52	12.3								
10.708	249.2	334.9	316.5	115.2	247	7.3	386.8	387.3	121.4	78	13.7								
11.346	257.2	233.5	217.9	61.8	261	3.8	271.7	250.8	81.8	86	8.8								
11.985	265.2	214.5	213.1	29.4	97	3.0	285.6	274.9	86.6	31	15.5								
12.623	273.2	223.9	216.3	45.9	51	6.4	293.6	295.2	64.6	24	13.2								
12.942	277.2	220.9	210.3	48.2	117	4.4	292.9	266.1	83.2	52	11.5	343.5	2	11.187	421.1	440.5	156.4	21	34.1

for *G. ruber* and *Orbulina universa* [*Bé and Duplessy*, 1976; *Hecht*, 1976], the latter species increased only slightly in size (Figure 3c). We therefore assume that absolute SST itself did not affect test size of *G. ruber*. This assumption is supported by the gradual decrease in test size at the end of sapropel S1, while SSTs remained generally stable (Figure 3) [*Castañeda et al.*, 2010].

Decreasing surface salinity due to excess river runoff in the early Holocene to mid-Holocene might have caused environmental stress to planktic foraminifers and might have led to the observed size change of *G. ruber* [e.g., *Rossignol-Strick et al.*, 1982; *Emeis et al.*, 2000]. A logical explanation for (1) increased average test size and (2) increased accumulation rates of *G. ruber* is provided by a mixed seasonal signal. Delayed reproduction during unfavorable conditions caused by high river runoff and freshened surface waters during summer monsoon is assumed to have impeded reproduction, and hence *G. ruber* might have grown larger over prolonged maturity [cf. *Schmidt et al.*, 2004b]. In turn, ameliorated conditions during the season of low river runoff (winter?) might have favored normal reproduction (fortnightly reproduction; cf. *Hemleben et al.* [1989]), leading to high accumulation rates of *G. ruber*. Reproduction could be also indicative of effects other than biological, including changes in the quantity and quality of food and changes in physical and chemical characteristics of the ambient seawater caused by changes in stratification of the surface water column [e.g., *Schmidt et al.*, 2004b].

In concordance with increasing primary production, increasing planktic foraminifer test sizes have been reported up to a threshold of 150 g C/m^2 a [*Faber et al.*, 1988; *Schmidt et al.*, 2004a]. Above this threshold value, the size of species decreases with increasing primary production. According to *Howell and Thunell* [1992] and *Emeis and Sakamoto* [1998], primary production during S1 was estimated at 393 g C/m^2 a and 200–1000 g C/m^2 a, respectively. Although these values have been much disputed, enhanced primary production during S1 may have had a negative effect on planktic foraminifer size. South of Cyprus (core SL9, 2302 m water depth; Figure 1), a decrease in test mass of *G. ruber* during sapropel S1 [*Principato et al.*, 2006] might seem contradictory to our results since both parameters (weight and size) often covary. However, this feature was attributed to dissolution relatively to the large water depth of the sediments analyzed by *Principato et al.* [2006]. In our shallow (552 m) water samples, calcite dissolution has not been observed, and even

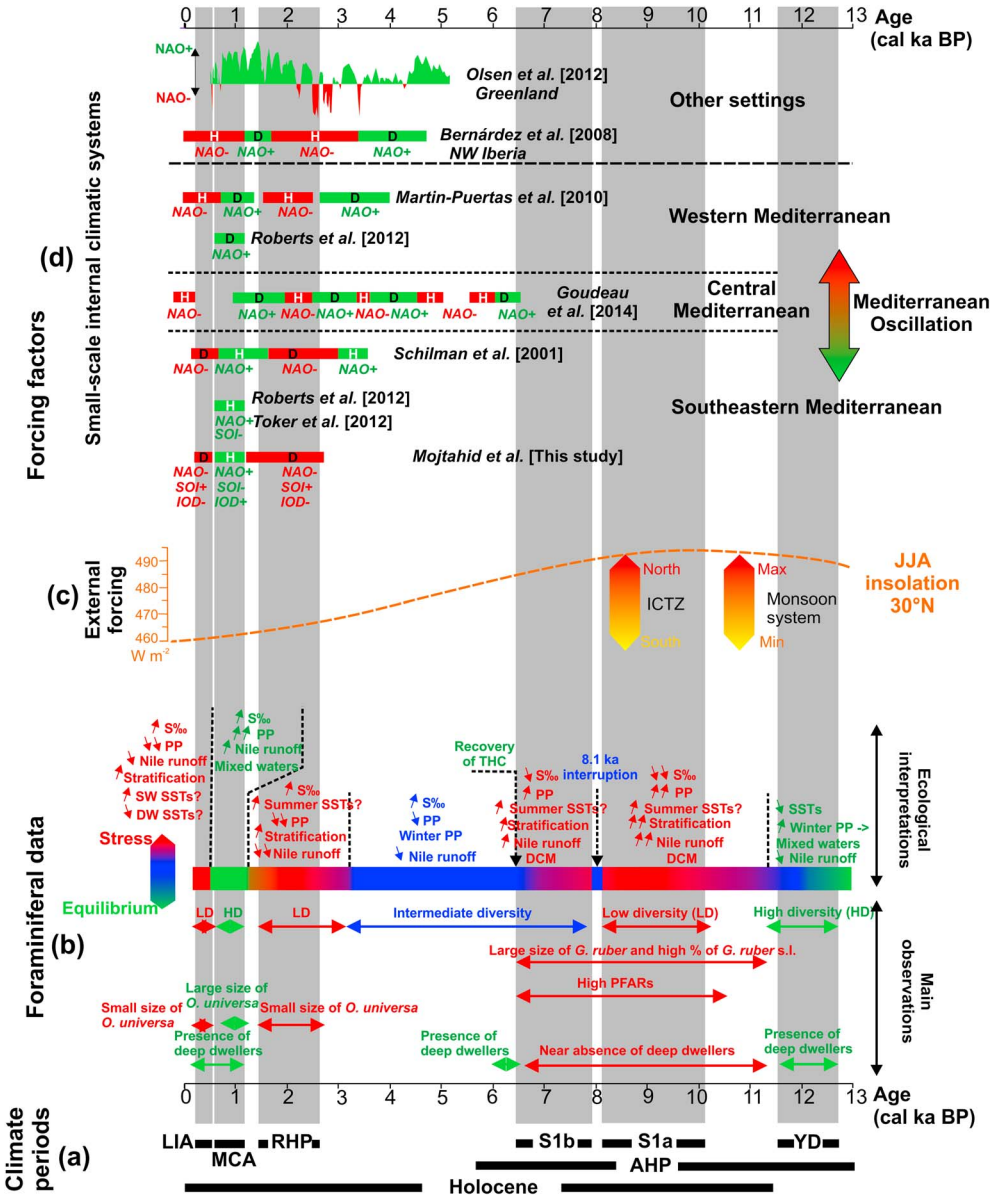

Figure 4. Summary scheme of the main results, paleoenvironmental reconstructions, and comparison to intervals/episodes defined from other proxies and by other authors at the regional to global scale. (a) Climate periods. (b) Summary scheme of the main foraminifer results and their environmental interpretations. PP: primary production; SSTs: sea surface temperatures; DCM: deep chlorophyll maximum; S: surface salinity; SW: surface waters (0–50 m); DW: deep waters (>200 m). (c) Summer insolation curve at 30°N [*Laskar et al.*, 2004] and the subsequent ITCZ positioning and monsoon intensity. (d) Holocene records of the discussed internal modes of climate variability (NAO, SOI, and IOD) in the eastern and western Mediterranean, Iberian Peninsula, and Greenland. The main events and climate phases are reported similarly to Figure 1.

aragonite (pteropod shells) is well preserved. In addition, decreasing foraminifer test mass in the early Holocene was shown to result from postglacial increase in atmospheric CO_2 concentration [*Barker and Elderfield*, 2002].

Therefore, the hypothesis of low-saline surface waters as main control of the size of *G. ruber* (white) during S1 in the southeastern Mediterranean appears to be the most plausible of explanations.

5.3. Effect of External Forcing on Nile River Discharge and Levantine Basin Surface Waters From Early Holocene to mid-Holocene, With Focus on sapropel S1 Formation

From the late Pleistocene to Holocene, orbital forcing controlled the relative northward position of the ITCZ. Maximum insolation due to Earth's orbital precession minimum significantly intensified the northeast

African monsoon, leading to enhanced discharge of fresh and nutrient-rich Nile River water into the eastern Mediterranean (Figure 4d) [e.g., *Rossignol-Strick et al*., 1982; *Emeis et al*., 2000]. The so-called African Humid Period started around 15.6 ka and hence before the record presented here [e.g., *Revel et al*., 2014], with an interruption to more arid conditions during the Younger Dryas (YD) cold event [*deMenocal et al*., 2000] (Figures 4a–4d).

The base of our record was deposited during the YD, well pronounced in North Atlantic climate records between ~12.9 and 11.7 cal ka B.P. [e.g., *Broecker*, 1994]. During the YD, faunal composition of planktic foraminifers indicated rather cold SSTs with a reduced contribution of *Globigerinoides ruber* and absence of the other subtropical and symbiont-bearing species as *G. ruber* pink and *Globigerinoides sacculifer* (Figure 2). The same was corroborated by SST estimates from a nearby core (GeoB 7702-3; Figures 1 and 2j) and the heavier values of $\delta^{18}O_{G.\ ruber}$ (Figure 2h) [*Castañeda et al*., 2010; *Hennekam et al*., 2014]. The effect of the YD climatic change initiated in the North Atlantic had well affected the southeastern Mediterranean [e.g., *Emeis et al*., 2000; *Almogi-Labin et al*., 2009; *Revel et al*., 2010]. *Lea et al*. [2003] suggested that meltwater input to the North Atlantic and collapse of the associated thermohaline circulation accompanied a southward shift of the ITCZ and consequent weakening of the monsoon system. During the same period of time, the foraminifer fauna of the Levantine was highly diverse (Figure 2b), and the abundance of opportunistic species like *Globigerina bulloides* indicated enhanced productivity of surface waters (Figures 2e and 4b). Enhanced productivity may be caused by the presence of (semi-) permanent eddies during winter and spring [*Pujol and Vergnaud-Grazzini*, 1995]. In the northern Levantine, *Abu-Zied et al*. [2008] deduced more productive water conditions from benthic foraminifer assemblages during the YD as well. Enhanced surface marine productivity during times of reduced African monsoon activity and reduced Nile River runoff would need an alternative nutrient source supporting primary production. *Robinson et al*. [2006] and *Box et al*. [2008] suggested intensified wind activity during the YD, fertilizing surface waters by aeolian sources, i.e., dust. In addition, enhanced surface water mixing and surface current activity (including eddies) might have caused entrainment of nutrients to surface waters. Reinforcement of hydrographic fronts may be indicated by enhanced numbers of *Globorotalia inflata*, which is assumed indicative of ecological conditions associated to oceanic fronts, and upwelling and downwelling activity. The presence of deep-dwelling *Globorotalia truncatulinoides* might even indicate reinforcement of subsurface currents in the Levantine Basin.

At the end of the YD event, gradual depletion of $\delta^{18}O_{G.\ ruber}$ and gradual increase in SSTs marked the onset of the Holocene around 11.5 cal ka B.P. (Figure 2). SST warming was indicated by decreasing numbers of *Neogloboquadrina pachyderma* and *N. incompta* and increasing numbers of *Globigerinoides ruber* white and pink. The occurrence of other subtropical and symbiont-bearing species like *Globigerinoides sacculifer* only ~800 years later may be due to increasing SSTs. The increase in the proportions of symbiont-bearing species, together with the gradual decrease in *Globigerina bulloides* and a drop in diversity, may mark a change to more oligotrophic conditions (Figures 2 and 4b). At the same time, excess Nile River runoff recorded under the humid climate at that time—the African Humid Period—might have resulted in low surface water salinity and hence unfavorable conditions for most planktic foraminifer species including *G. bulloides*. Because enhanced fresh water input affects the survival of most species, and introduces light $\delta^{13}C$ terrestrial carbon, neither composition of the planktic foraminifer assemblage nor $\delta^{13}C_{G.\ ruber}$ can provide accurate information about surface productivity in this climatic context. Furthermore, the decrease of the $\delta^{13}C$ signal during S1 could be partly explained through closer equilibrium with the atmosphere (i.e., more stratified and maybe warmer waters). It is yet interesting to note the high proportions of *G. ruber* white (s.l.) and the increase in PFAR values, which indicate enhanced surface productivity as discussed in section 5.1. Concomitantly, the decline in the proportions of deep dwellers marked gradual water column stratification (Figure 2g). In conclusion, our planktic foraminifer record indicates a gradual increase in water column stratification and surface productivity, both preceding the deposition of the anoxic sapropel S1 layer (Figure 4b). This might suggest that it takes several hundred years and water column stratification to consume most oxygen through this increase in productivity.

Within the sapropel S1 event (~10.1–6.4 cal ka B.P.), the distribution of planktic foraminifers seemed to be represented by two major phases with a transitional phase from ~8.8–8.0 ka (Figures 2 and 4). These two phases corresponded mostly to S1a and S1b events determined from geochemical properties measured in the same core and interrupted by S1/oxidized S1 limit around 8.1 ka (Figure 2) [*Hennekam et al*., 2014]. A severe drop in planktic foraminifer diversity in the earlier phase indicates ecological conditions which were

limiting to the abundance of some species and less so to others (Figure 2b). The drop in diversity was marked by the dominance of *Globigerinoides ruber*, while most other planktic foraminifer species almost disappeared. Interestingly, the interval of lowest salinity went along with the most depleted $\delta^{18}O_{G.\ ruber}$ (Figure 2h), and the highest Ba/Ca values of *G. ruber* [*Weldeab et al*., 2014]. At ~8.8 cal ka B.P., a dip in PFAR possibly indicated reduced productivity. Although some species such as *Globigerinoides sacculifer* started to slightly increase in proportions, and *G. ruber* (particularly *G. ruber* s.s.) started decreasing in size at that time (Figures 2d, 3a, and 3b), the temporal resolution of our record does not allow evoking a clear ecological change at ~8.8 cal ka B.P. Therefore, we are hesitant to interpret the decreased PFAR values as a productivity decrease, especially as Ba/Al (export productivity proxy) and organic carbon stayed relatively constant throughout this time interval [*Hennekam et al*., 2014].

Another decrease in PFAR values, recorded around 8.0–8.1 ka, coincides with the S1/oxidized S1 limit (S1a/S1b) defined from sediment characteristics in the same core and elsewhere in the eastern Mediterranean (Figure 2) [*Hennekam et al*., 2014]. Most studies have related the S1 interruption to the Northern Hemisphere 8.2 cold event and a collapse in North Atlantic thermohaline circulation caused by the drainage of melt waters from North American proglacial lakes [e.g., *Rohling and Pälike*, 2005]. In the Aegean Sea, the 8.2 event was further attributed to a more pronounced Siberian high-pressure system involving cooler temperatures [e.g., *Pross et al*., 2009] and to a southward migration of the ITCZ weakening the monsoon systems [e.g., *Fleitmann et al*., 2007]. Our PFAR values indicate that productivity was reduced during this time although above background values (Figure 2a). As PFAR is less influenced by preservation than most other productivity proxies (e.g., Dinocysts) [*Zonneveld et al*., 2001], we assume that the cold event around 8.2 ka did not only affect the benthic (foraminifer) fauna [e.g., *Schmiedl et al*., 2003] but also surface water conditions in the eastern Mediterranean.

After the ~8.8–8.0 ka transition phase, the return to high PFARs reflects a return to stressful ecological conditions that was less dramatic for planktic fauna than during the first phase (Figure 4b). In fact, the S1b interval differed clearly from S1a in that *G. sacculifer* were present in larger numbers, while *G. ruber* percentages were lower. This probably relates to enhanced salinity and lower freshwater discharge from the Nile River. Stratification of the water column may have decreased at the same time, leading to less limiting conditions and a more diverse planktic foraminifer assemblage. This change in environmental conditions paralleled the increase in $\delta^{13}C$ and $\delta^{18}O$ values of *G. ruber* marking the progressive decrease in Nile River runoff as stated by *Hennekam et al*. [2014] and *Weldeab et al*. [2014], at decreasing insolation.

5.4. Imprint of Internal Modes of Climate Variability From the mid-Holocene to Late Holocene

At the end of S1, planktic foraminifer data indicate a return to pre-S1 conditions. Planktic foraminifer accumulation rates decreased, and the test size of *Globigerinoides ruber* decreased to pre-S1 values. A characteristic peak of *Globorotalia inflata* indicates decreasing surface water stratification and the recovery of thermohaline circulation (Figure 2g) [e.g., *Casford et al*., 2002; *Capotondi et al*., 2006; *Principato et al*., 2006]. Those changes are discussed to result from a southward shift of the ITCZ initiating a period of progressive aridification in the Levantine region [e.g., *Bar-Matthews et al*., 2003]. The significant decrease in Nile River runoff allowed for higher foraminifer diversity. In this context, *G. ruber* was no longer exposed to low-saline waters resulting from Nile runoff. Therefore, after S1 time period, *G. ruber* resumed an ecological niche similar to the modern one, i.e., the oligotophic waters of the eastern Mediterranean Sea.

Until ~2.9 cal ka B.P., progressively decreasing proportions of the deepest surface morphotype s.l. of *G. ruber* white might indicate lower nutrient input and thus decreasing primary production. By being less charged by continental carbon sources, the diminishing $\delta^{13}C_{G.\ ruber}$ values might also indicate decreasing productivity. This is consistent with the progressive, southward retreat of the ITCZ, in line with a reduced river-derived flux of nutrients and thus a weakening of ocean fertilization. Reoccurrence of *Globigerina bulloides* and intermediate planktic foraminifer diversity recorded after S1 suggests moderately productive surface waters. Because insolation (external forcing) was gradually decreasing (Figure 2i) during this time period, the imprint of "internal" variability of the coupled ocean-atmosphere system should be more perceptible as suggested by *Debret et al*. [2009] (Figures 4c and 4d). One facet of this shift can be seen in the general surface water warming recorded by *Castañeda et al*. [2010] (Figure 2j) in opposite to the North Atlantic Ocean and the western Mediterranean [e.g., *Kim et al*., 2004; *Castañeda et al*., 2010], which seems counterinductive in this general context of decreasing insolation. To explain this seesaw, *Kim et al*. [2004] suggested oceanic and atmospheric teleconnections to, for instance, the North Atlantic Oscillation (NAO) and Pacific Decadal Oscillation.

From ~2.9 to 1.1 cal ka B.P., the decrease in planktic foraminifer diversity was mainly due to an increase in *G. ruber* white (Figures 3b, 3c, and 4a), possibly caused by oligotrophic conditions to which this species is well adapted. Intense aridification prevailed in the eastern Mediterranean around this time period and in the Nile catchment area around 3–2 cal ka B.P. [*Schilman et al*., 2001; *Revel et al*., 2014]. Because $\delta^{13}C_{G.\ ruber}$ did not show a clear pattern, we assume that arid conditions were more pronounced during summers (*G. ruber* being a summer species), whereas the presence of the eutrophic species *Globigerina bulloides* (winter species) indicated rather productive surface waters. Accentuated seasonality was also pointed out by *Castañeda et al*. [2010] discussing the incongruity between TEX_{86} and $U^{k'}_{37}$ values at ~1.9 cal ka B.P. explaining warmer summers (Figure 2j). Additionally, *Orbulina universa* was smaller during this time period (Figure 3) possibly reflecting an environmental change and probably more oligotrophic conditions. Dryer conditions in the Levantine region may have led to higher evaporation, which could explain the slightly heavier values of $\delta^{18}O_{G.\ ruber}$ (Figure 2). It is interesting to note that the arid conditions coincided with the Roman Humid Period (~2.6–1.6 cal ka B.P.) well recorded in the North Atlantic and western Mediterranean under a predominantly negative NAO state, i.e., more humid conditions [e.g., *Cullen and deMenocal*, 2000; *Mojtahid et al*., 2013]. It has been suggested that NAO affects eastern Mediterranean ecosystems in antiphase with western Mediterranean precipitation and atmospheric pressure [e.g., *Oldfield and Thompson*, 2004; *Xoplaki et al*., 2004; *Roberts et al*., 2012]. Those conditions are discussed as Mediterranean Oscillation by *Conte et al*. [1989]. Although such aridification might have affected small rivers in the Levant, the main source of freshwater and nutrients to our coring site remains the Nile River. What could therefore be the direct cause of lower Nile River discharge resulting in oligotrophic southeastern Mediterranean waters as revealed by planktic foraminifers during this time interval? Nile River runoff is not directly linked to NAO as the Nile catchment area is dominated by precipitation linked with the monsoon system, which in turn is affected by southern atmospheric systems such as the Indian Ocean Dipole (IOD) [*Saji et al*., 1999]. Under recent pre-Aswan values, the El Niño/La Niña-Southern Oscillation (ENSO) was discussed to have accounted for 25% of the variability of the annual Nile River runoff [*Eltahir*, 1996]. A connection between NAO and ENSO was proposed, as well as a positive state of NAO coinciding with a negative Southern Oscillation Index (SOI) [*Marriner et al*., 2012; *Toker et al*., 2012] (Figure 4d).

From ~1.1 to 0.54 cal ka B.P., relative decrease in *G. ruber* and other symbiont-bearing species (except of *G. sacculifer*) and increase in opportunistic species like *G. bulloides* reflect more productive surface waters. As a result, a significant increase in diversity indicated more favorable and equilibrated ecological conditions in surface waters. Increased humidity in the region was documented by an increase of Nile River runoff. Even in northwestern India, humid conditions prevailed during this time period [*Nicholson*, 1980; *Singh et al*., 1990; *Schilman et al*., 2001]. Wetter regional conditions probably occurred all over the Middle East, suggesting that the local southeastern Mediterranean rainfall simultaneously increased with an enhanced monsoonal activity that recharged the Nile headwaters. An increase in riverine nutrient load might have favored the development of opportunistic taxa without exerting a negative effect on planktic species through lowering salinity. The size of *Orbulina universa* reached a maximum during this time period, perhaps reflecting optimum ecological growth conditions (Figure 3c). The occurrence of the symbiont-bearing *G. sacculifer* in high proportions may seem contradictory. However, since the latter is nowadays nearly absent from the modern planktic assemblage of the oligotrophic Levantine Basin and mostly present in the more fertile western Mediterranean [*Pujol and Vergnaud-Grazzini*, 1995], we assume that this species might be sensitive to extreme nutrient-limiting and prefers more nutrient-rich surface waters. It is interesting to note that this time interval, including the "Medieval Climate Anomaly" (MCA) period, coincides with a positive NAO and negative SOI conditions [*Toker et al*., 2012] (Figure 4). This might corroborate the NAO-Mediterranean seesaw [e.g., *Martín-Puertas et al*., 2010] and a possible link to southern climate systems like the Indian Ocean Dipole (IOD) and probably ENSO.

From ~0.54 cal ka B.P. until the end of record (excluding the last 0.16 ka characterized by three very poor samples; Table 1), a major drop in diversity, diminishing proportions of opportunistic *G. bulloides*, low $\delta^{13}C_{G.\ ruber}$, and size decrease of *O. universa* indicate another period of aridity and prevailing oligotrophic conditions (Figure 4d). Additionally, *G. ruber* pink attained high faunal portions of up to ~20% for the first time in our record. Such a planktic foraminifer assemblage, mainly composed of *G. ruber* white and pink, is similar to modern summer assemblages in the more oligotrophic settings south of Cyprus [*Pujol and Vergnaud-Grazzini*, 1995] (Figure 1). In fact, this period encompassed another historic Northern Hemisphere cooling event known as the Little Ice Age (LIA) from the fifteenth to nineteenth centuries, i.e., about 0.6–0.2 cal ka B.P. [*Roberts et al*., 2012]. Climate data for this time period in the Levant are scarce and generally disagree with

the response of the eastern Mediterranean climate to global LIA conditions. Most regional studies report drier conditions [e.g., *Schilman et al*., 2001, 2002; *Bar-Matthews et al*., 2003; *Jones et al*., 2006; *Griggs et al*., 2007]. Decreased precipitation in Central Asia due to a weaker Indian monsoon might explain this general aridity causing reduced Nile River runoff [*Kaniewski et al*., 2011, and references therein]. The major disagreement remains on whether colder [*Bar-Matthews et al*., 1998; *Schilman et al*., 2001; *Kaniewski et al*., 2011] or warmer climate conditions [*Roberts et al*., 2012; *Wanner et al*., 2008] prevailed. The latter authors suggest an effect of the east-west climate seesaw from negative NAO conditions (Figure 4d). The answer from our planktic record is not very clear, though. The presence of *G. ruber* pink suggests warmer SSTs, whereas the disappearance of *G. sacculifer* seems not to be caused by changing temperature but nutrient limitation. The occurrence of the cold water taxon *Neogloboquadrina pachyderma* together with *G. ruber* pink is assumed to display seasonality, with *G. ruber* pink being a summer species living in surface waters and *N. pachyderma* a winter deep-dwelling species living at or below the thermocline (>200 m) in the eastern Mediterranean [*Pujol and Vergnaud-Grazzini*, 1995]. We assume that the general aridity prevailing during the LIA and increased evaporation during summer may have reinforced thermohaline circulation. Deep waters were possibly colder than before and were formed in northern basins (e.g., Aegean Sea) subjected to climate cooling. On the contrary, surface waters in the eastern Mediterranean may have experienced a general warming.

6. Conclusions

Climate in the eastern Mediterranean over the past 13 cal ka B.P. was mainly forced by changes in insolation. The resulting position of the ITCZ controlled the monsoon system, which in turn controlled Nile River runoff and thus fresh water discharge and nutrient input into the southeastern Levantine Basin. Variations of Nile River discharge directly affected surface water conditions in the region of our coring site, i.e., salinity and nutrient fluxes, hence controlling the development of the planktic foraminifer fauna.

Although Nile River runoff decreased during the Younger Dryas as a result of a southward migration of the ITCZ, the high diversity of the planktic foraminifer assemblage, the presence of the opportunistic *Globigerina bulloides*, and the dominance of deep dwellers indicate increased productivity in a well-mixed water column. From the early Holocene to ~6.4 cal ka B.P., the northward shift of the ITCZ may have reinforced the monsoon system and enhanced Nile River runoff. This resulted in an increased water column stratification leading to the deposition of sapropel S1. High accumulation rates of planktic foraminifers indicate enhanced primary production. The predominant presence of large-sized specimens of the more euryhaline *Globigerinoides ruber* indicate low-saline waters. At 6.4 cal ka B.P., the deep dweller *Globorotalia inflata* marked the breaking up of stratification and the recovery of thermohaline circulation. Because the Nile runoff significantly decreased in parallel to the southward shift of the ITCZ, a more diverse planktic community was found, with *G. ruber* thriving under oligotophic conditions. The last 2.9 ka encompassed a succession of three ecosystem states characterized by nutrient-limiting surface waters from 2.9 to 1.1 ka and 0.54 to 0.1 ka (LIA) and by nutrient-rich waters from 1.1 to 0.54 ka (MCA). Those conditions were linked to periods of low and high Nile River runoff, respectively, in line with arid and humid climate conditions in the Levant and Nile headwaters. In accordance with literature, we conclude that humidity of the Levantine region was predominantly affected by the NAO over the past 2.9 ka. In addition to precipitation in eastern Mediterranean, surface salinity was affected by monsoonal activity, i.e., Southern Oscillation and the Indian Ocean Dipole and precipitation in the Nile catchment area, which recharged the Nile headwaters and fueled Nile River runoff. Conditions in the eastern and western Mediterranean were in antiphase, and the Mediterranean oscillation proposed by *Conte et al*. [1989] is confirmed by our results.

Acknowledgments

This study is part of a project MADHO (MediterraneAn Deltas in the Holocene) financed by the international program MISTRALS PaleoMEX. A 5 month MSc fellowship was provided to Rose Manceau to perform this study. NWO is acknowledged for financial support to PASSAP cruise and PASS2 and PALM projects. Data to support this article are from University of Angers (France) and University of Utrecht (The Netherlands). The data are available by contacting the first author (e-mail: meryem.mojtahid@univ-angers.fr).

References

Abu-Zied, R. H., E. J. Rohling, F. J. Jorissen, C. Fontanier, J. S. L. Casford, and S. Cooke (2008), Benthic foraminiferal response to changes in bottom-water oxygenation and organic carbon flux in the eastern Mediterranean during LGM to recent times, *Mar. Micropaleontol.*, *67*, 46–68, doi:10.1016/j.marmicro.2007.08.006.

Almogi-Labin, A., M. Bar-Matthews, D. Shriki, E. Kolosovsky, M. Paterne, B. Schilman, A. Ayalon, Z. Aizenshtat, and A. Matthews (2009), Climatic variability during the last ~ 90 ka of the southern and northern Levantine Basin as evident from marine records and speleothems, *Quat. Sci. Rev.*, *28*, 2882–2896, doi:10.1016/j.quascirev.2009.07.017.

Barker, S., and H. Elderfield (2002), Foraminiferal calcification response to glacial-interglacial changes in atmospheric CO_2, *Science*, *297*, 833–836.

Bar-Matthews, M., and A. Ayalon (2011), Mid-Holocene climate variations revealed by high-resolution speleothem records from Soreq Cave, Israel and their correlation with cultural changes, *Holocene*, *21*, 163–171, doi:10.1177/0959683610384165.

Bar-Matthews, M., A. Ayalon, and A. Kaufman (1998), Middle to late Holocene (6,500 yr. period) paleoclimate in the Eastern Mediterranean Region from stable isotopic composition of speleothems from Soreq Cave, Israel, in *Water, Environment and Society in Times of Climatic Change*, *Water Sci. Technol. Lib.*, edited by A. S. Issar and N. Brown, pp. 203–214, Springer, Netherlands.

Bar-Matthews, M., A. Ayalon, A. Kaufman, and G. J. Wasserburg (1999), The Eastern Mediterranean paleoclimate as a reflection of regional events: Soreq cave, Israel, *Earth Planet. Sci. Lett.*, *166*, 85–95, doi:10.1016/S0012-821X(98)00275-1.

Bar-Matthews, M., A. Ayalon, M. Gilmour, A. Matthews, and C. J. Hawkesworth (2003), Sea–land oxygen isotopic relationships from planktonic foraminifera and speleothems in the Eastern Mediterranean region and their implication for paleorainfall during interglacial intervals, *Geochim. Cosmochim. Acta*, *67*, 3181–3199, doi:10.1016/S0016-7037(02)01031-1.

Bé, A. W. H., and J.-C. Duplessy (1976), Subtropical convergence fluctuations and Quaternary climates in the middle latitudes of the Indian Ocean, *Science*, *194*, 419–422, doi:10.1126/science.194.4263.419.

Bé, A. W. H., and D. S. Tolderlund (1971), Distribution and ecology of living planktonic foraminifera in surface waters of the Atlantic and Indian Oceans, in *The Micropaleontology of the Oceans*, edited by B. M. Funnel and W. R. Riedel, pp. 105–149, Cambridge Univ. Press, Cambridge, U. K.

Beer, C. J., R. Schiebel, and P. A. Wilson (2010), Testing planktic foraminiferal shell weight as a surface water [CO_3^{2-}] proxy using plankton net samples, *Geology*, *38*, 103–106, doi:10.1130/G30150.1.

Bijma, J., W. W. Faber, and C. Hemleben (1990), Temperature and salinity limits for growth and survival of some planktonic foraminifers in laboratory cultures, *J. Foraminifer. Res.*, *20*, 95–116.

Bollmann, J., P. S. Quinn, M. Vela, B. Brabec, S. Brechner, M. Y. Cortes, H. Hilbrecht, D. N. Schmidt, R. Schiebel, and H. R. Thierstein (2004), Automated particle analysis: Calcareous microfossils, in *Image Analysis, Sediments and Paleoenvironments*, edited by P. Francus, pp. 229–252, Kluwer Acad., Dordrecht, Netherlands.

Bottema, S. (1995), The Younger Dryas in the Eastern Mediterranean, *Quat. Sci. Rev.*, *14*, 883–891, doi:10.1016/0277-3791(95)00069-0.

Box, M. R., M. D. Krom, R. Cliff, A. Almogi-Labin, M. Bar-Matthews, A. Ayalon, B. Schillman, and M. Paterne (2008), Changes in the flux of Saharan dust to the East Mediterranean Sea since the last glacial maximum as observed through Sr-isotope geochemistry, *Mineral. Mag.*, *72*, 307–311, doi:10.1180/minmag.2008.072.1.307.

Box, M. R., M. D. Krom, R. A. Cliff, M. Bar-Matthews, A. Almogi-Labin, A. Ayalon, and M. Paterne (2011), Response of the Nile and its catchment to millennial-scale climatic change since the LGM from Sr isotopes and major elements of East Mediterranean sediments, *Quat. Sci. Rev.*, *30*, 431–442, doi:10.1016/j.quascirev.2010.12.005.

Broecker, W. S. (1994), Massive iceberg discharges as triggers for global climate change, *Nature*, *372*, 421–424, doi:10.1038/372421a0.

Capotondi, L., A. M. Borsetti, and C. Morigi (1999), Foraminiferal ecozones, a high resolution proxy for the late Quaternary biochronology in the central Mediterranean Sea, *Mar. Geol.*, *153*, 253–274, doi:10.1016/S0025-3227(98)00079-6.

Capotondi, L., M. S. Principato, C. Morigi, F. Sangiorgi, P. Maffioli, S. Giunta, A. Negri, and C. Corselli (2006), Foraminiferal variations and stratigraphic implications to the deposition of sapropel S5 in the eastern Mediterranean, *Palaeogeogr. Palaeoclimatol. Palaeoecol.*, *235*, 48–65, doi:10.1016/j.palaeo.2005.09.023.

Casford, J. S. L., E. J. Rohling, R. Abu-Zied, S. Cooke, C. Fontanier, M. Leng, and V. Lykousis (2002), Circulation changes and nutrient concentrations in the late Quaternary Aegean Sea: A nonsteady state concept for sapropel formation, *Paleoceanography*, *17*, 14–1, doi:10.1029/2000PA000601.

Castañeda, I. S., E. Schefuß, J. Pätzold, J. S. Sinninghe Damsté, S. Weldeab, and S. Schouten (2010), Millennial-scale sea surface temperature changes in the eastern Mediterranean (Nile River delta region) over the last 27,000 years, *Paleoceanography*, *25*, PA1208, doi:10.1029/2009PA001740.

Conte, M., S. Giuffrida, and S. Tedesco (1989), The Mediterranean oscillation impact on precipitation and hydrology in Italy, in *Proceedings Conference Climate Water*, vol. 1, pp. 121–137, Publications of Academy of Finland, Helsinki.

Cullen, H. M., and P. B. deMenocal (2000), North Atlantic influence on Tigris–Euphrates streamflow, *Int. J. Climatol.*, *20*, 853–863, doi:10.1002/1097-0088(20000630)20:8<853::AID-JOC497>3.0.CO;2-M.

De Lange, G. J., J. Thomson, A. Reitz, C. P. Slomp, M. Speranza Principato, E. Erba, and C. Corselli (2008), Synchronous basin-wide formation and redox-controlled preservation of a Mediterranean sapropel, *Nat. Geosci.*, *1*, 606–610, doi:10.1038/ngeo283.

Debret, M., D. Sebag, X. Crosta, N. Massei, J.-R. Petit, E. Chapron, and V. Bout-Roumazeilles (2009), Evidence from wavelet analysis for a mid-Holocene transition in global climate forcing, *Quat. Sci. Rev.*, *28*, 2675–2688, doi:10.1016/j.quascirev.2009.06.005.

deMenocal, P., J. Ortiz, T. Guilderson, J. Adkins, M. Sarnthein, L. Baker, and M. Yarusinsky (2000), Abrupt onset and termination of the African humid period: Rapid climate responses to gradual insolation forcing, *Quat. Sci. Rev.*, *19*, 347–361, doi:10.1016/S0277-3791(99)00081-5.

Ducassou, E., T. Mulder, S. Migeon, E. Gonthier, A. Murat, M. Revel, L. Capotondi, S. M. Bernasconi, J. Mascle, and S. Zaragosi (2008), Nile floods recorded in deep Mediterranean sediments, *Quat. Res.*, *70*, 382–391, doi:10.1016/j.yqres.2008.02.011.

Eltahir, E. A. B. (1996), El Niño and the natural variability in the flow of the Nile River, *Water Resour. Res.*, *32*, 131–137, doi:10.1029/95WR02968.

Emeis, K.-C., and T. Sakamoto (1998), The sapropel theme of leg 160, in *Proceedings of the Ocean Drilling Program*, *Sci. Results*, vol. 160, edited by A. H. F. Robertson et al., pp. 29–36, Ocean Drill. Program, College Station, Tex.

Emeis, K.-C., U. Struck, H.-M. Schulz, R. Rosenberg, S. Bernasconi, H. Erlenkeuser, T. Sakamoto, and F. Martinez-Ruiz (2000), Temperature and salinity variations of Mediterranean Sea surface waters over the last 16,000 years from records of planktonic stable oxygen isotopes and alkenone unsaturation ratios, *Palaeogeogr. Palaeoclimatol. Palaeoecol.*, *158*, 259–280, doi:10.1016/S0031-0182(00)00053-5.

Eshel, G. (2002), Mediterranean climates, *Isr. J. Earth Sci.*, *51*, 157–168.

Faber, W. W., O. R. Anderson, J. L. Lindsey, and D. A. Caron (1988), Algal-foraminiferal symbiosis in the planktonic foraminifer *Globigerinella aequilateralia*; I, Occurrence and stability of two mutually exclusive chrysophyte endosymbionts and their ultrastructure, *J. Foraminifer. Res.*, *18*, 334–343, doi:10.2113/gsjfr.18.4.334.

Fleitmann, D., et al. (2007), Holocene ITCZ and Indian monsoon dynamics recorded in stalagmites from Oman and Yemen (Socotra), *Quat. Sci. Rev.*, *26*, 170–188, doi:10.1016/j.quascirev.2006.04.012.

Gasse, F. (2000), Hydrological changes in the African tropics since the Last Glacial Maximum, *Quat. Sci. Rev.*, *19*, 189–211, doi:10.1016/S0277-3791(99)00061-X.

Griggs, C., A. DeGaetano, P. Kuniholm, and M. Newton (2007), A regional high-frequency reconstruction of May–June precipitation in the north Aegean from oak tree rings, A.D. 1089–1989, *Int. J. Climatol.*, *27*, 1075–1089, doi:10.1002/joc.1459.

Hamann, Y., W. Ehrmann, G. Schmiedl, and T. Kuhnt (2009), Modern and late Quaternary clay mineral distribution in the area of the SE Mediterranean Sea, *Quat. Res.*, *71*, 453–464, doi:10.1016/j.yqres.2009.01.001.

Hecht, A. D. (1976), An ecologic model for test size variation in recent planktonic foraminifera; applications to the fossil record, *J. Foraminifer. Res.*, *6*, 295–311, doi:10.2113/gsjfr.6.4.295.

Hemleben, C., M. Spindler, and O. R. Anderson (Eds.) (1989), *Modern Planktonic Foraminifera*, Springer, New York.
Hennekam, R., and G. J. de Lange (2012), X-ray fluorescence core scanning of wet marine sediments: Methods to improve quality and reproducibility of high-resolution paleoenvironmental records, *Limnol. Oceanogr. Methods*, *10*, 991–1003, doi:10.4319/lom.2012.10.991.
Hennekam, R., T. Jilbert, B. Schnetger, and G. J. de Lange (2014), Solar forcing of Nile discharge and sapropel S1 formation in the early to middle Holocene eastern Mediterranean, *Paleoceanography*, 343–356, doi:10.1002/2013PA002553.
Howell, M. W., and R. C. Thunell (1992), Organic carbon accumulation in Bannock Basin: Evaluating the role of productivity in the formation of eastern Mediterranean sapropels, *Mar. Geol.*, *103*, 461–471, doi:10.1016/0025-3227(92)90032-D.
Incarbona, A., P. Ziveri, N. Sabatino, D. S. Manta, and M. Sprovieri (2011), Conflicting coccolithophore and geochemical evidence for productivity levels in the Eastern Mediterranean sapropel S1, *Mar. Micropaleontol.*, *81*, 131–143, doi:10.1016/j.marmicro.2011.09.003.
IPCC (2013), Climate Change 2013. The Physical Science Basis Working Group 1 Contribution to the fifth assessment report of the intergovernmental panel on climate change.
Issar, A. (2003), *Climate Changes During the Holocene and Their Impact on Hydrological Systems*, Cambridge Univ. Press, Cambridge, U. K.
Jones, M. D., C. N. Roberts, M. J. Leng, and M. Türkeş (2006), A high-resolution late Holocene lake isotope record from Turkey and links to North Atlantic and monsoon climate, *Geology*, *34*, 361, doi:10.1130/G22407.1.
Jorissen, F. J., A. Asioli, A. M. Borsetti, L. Capotondi, J. P. de Visser, F. J. Hilgen, E. J. Rohling, K. van der Borg, C. Vergnaud Grazzini, and W. J. Zachariasse (1993), Late Quaternary central Mediterranean biochronology, *Mar. Micropaleontol.*, *21*, 169–189, doi:10.1016/0377-8398(93)90014-O.
Kallel, N., M. Paterne, J.-C. Duplessy, C. Vergnaud-Grazzini, C. Pujol, L. Labeyrie, M. Arnold, M. Fontugne, and C. Pierre (1997), Enhanced rainfall in the Mediterranean region during the last sapropel event, *Oceanol. Acta*, *20*, 697–712.
Kaniewski, D., E. Van Campo, E. Paulissen, H. Weiss, J. Bakker, I. Rossignol, and K. Van Lerberghe (2011), The medieval climate anomaly and the Little Ice Age in coastal Syria inferred from pollen-derived palaeoclimatic patterns, *Global Planet. Change*, *78*, 178–187, doi:10.1016/j.gloplacha.2011.06.010.
Kim, J.-H., N. Rimbu, S. J. Lorenz, G. Lohmann, S.-I. Nam, S. Schouten, C. Rühlemann, and R. R. Schneider (2004), North Pacific and North Atlantic sea-surface temperature variability during the Holocene, *Quat. Sci. Rev.*, *23*, 2141–2154, doi:10.1016/j.quascirev.2004.08.010.
Kress, N., I. Gertman, and B. Herut (2014), Temporal evolution of physical and chemical characteristics of the water column in the easternmost Levantine basin (Eastern Mediterranean Sea) from 2002 to 2010, *J. Mar. Syst.*, *135*, 6–13, doi:10.1016/j.jmarsys.2013.11.016.
Krom, M. D., R. A. Cliff, L. M. Eijsink, B. Herut, and R. Chester (1999), The characterisation of Saharan dusts and Nile particulate matter in surface sediments from the Levantine basin using Sr isotopes, *Mar. Geol.*, *155*, 319–330, doi:10.1016/S0025-3227(98)00130-3.
Laskar, J., P. Robutel, F. Joutel, M. Gastineau, A. C. M. Correia, and B. Levrard (2004), A long-term numerical solution for the insolation quantities of the Earth, *Astron. Astrophys.*, *428*, 261–285.
Lea, D. W., D. K. Pak, L. C. Peterson, and K. A. Hughen (2003), Synchroneity of tropical and high-latitude Atlantic temperatures over the Last Glacial Termination, *Science*, *301*, 1361–1364, doi:10.1126/science.1088470.
Luz, B., and M. Bernstein (1976), Planktonic foraminifera and quantitative paleoclimatology of the Eastern Mediterranean, *Mar. Micropaleontol.*, *1*, 307–323, doi:10.1016/0377-8398(76)90014-1.
Marriner, N., C. Flaux, D. Kaniewski, C. Morhange, G. Leduc, V. Moron, Z. Chen, F. Gasse, J.-Y. Empereur, and J.-D. Stanley (2012), ITCZ and ENSO-like pacing of Nile delta hydro-geomorphology during the Holocene, *Quat. Sci. Rev.*, *45*, 73–84, doi:10.1016/j.quascirev.2012.04.022.
Martín-Puertas, C., F. J. Jimenez Espejo, F. Martínez-Ruiz, V. Nieto-Moreno, M. Rodrigo, M. P. Mata, and B. L. Valero-Garcés (2010), Late Holocene climate variability in the southwestern Mediterranean region: An integrated marine and terrestrial geochemical approach, *Clim. Past*, *6*, 807–816, doi:10.5194/cp-6-807-2010.
Marullo, S., R. Santoleri, P. Malanotte-Rizzoli, and A. Bergamasco (1999), The sea surface temperature field in the Eastern Mediterranean from advanced very high resolution radiometer (AVHRR) data, *J. Mar. Syst.*, *20*, 83–112, doi:10.1016/S0924-7963(98)00072-4.
Mojtahid, M., et al. (2013), High resolution Holocene record in the southeastern Bay of Biscay: Global versus regional climate signals, *Palaeogeogr. Palaeoclimatol. Palaeoecol.*, *377*, 28–44, doi:10.1016/j.palaeo.2013.03.004.
Myers, P. G., K. Haines, and E. J. Rohling (1998), Modeling the paleocirculation of the Mediterranean: The last glacial maximum and the Holocene with emphasis on the formation of sapropel S1, *Paleoceanography*, *13*, 586–606, doi:10.1029/98PA02736.
Naidu, P. D., and B. A. Malmgren (1995), Monsoon upwelling effects on test size of some planktonic foraminiferal species from the Oman Margin, Arabian Sea, *Paleoceanography*, *10*, 117–122, doi:10.1029/94PA02682.
Nicholson, S. (1980), Saharan climates in historic times, in *The Sahara and the Nile*, edited by M. A. J. Williams and H. Faure, pp. 173–200, A.A. Balkema, Rotterdam.
Oldfield, F., and R. Thompson (2004), Archives and proxies along the PEP III transect, in *Past Climate Variability through Europe and Africa*, *Dev. in Paleoenviron. Res.*, edited by R. W. Battarbee, F. Gasse, and C. E. Stickley, pp. 7–29, Springer, Netherlands.
Orland, I. J., M. Bar-Matthews, A. Ayalon, A. Matthews, R. Kozdon, T. Ushikubo, and J. W. Valley (2012), Seasonal resolution of Eastern Mediterranean climate change since 34 ka from a Soreq Cave speleothem, *Geochim. Cosmochim. Acta*, *89*, 240–255, doi:10.1016/j.gca.2012.04.035.
Principato, M. S., S. Giunta, C. Corselli, and A. Negri (2003), Late Pleistocene–Holocene planktonic assemblages in three box-cores from the Mediterranean Ridge area (west–southwest of Crete): Palaeoecological and palaeoceanographic reconstruction of sapropel S1 interval, *Palaeogeogr. Palaeoclimatol. Palaeoecol.*, *190*, 61–77, doi:10.1016/S0031-0182(02)00599-0.
Principato, M. S., D. Crudeli, P. Ziveri, C. P. Slomp, C. Corselli, E. Erba, and G. J. de Lange (2006), Phyto_ and zooplankton paleofluxes during the deposition of sapropel S1 (eastern Mediterranean): Biogenic carbonate preservation and paleoecological implications, *Palaeogeogr. Palaeoclimatol. Palaeoecol.*, *235*, 8–27, doi:10.1016/j.palaeo.2005.09.021.
Pross, J., U. Kotthoff, U. C. Müller, O. Peyron, I. Dormoy, G. Schmiedl, S. Kalaitzidis, and A. M. Smith (2009), Massive perturbation in terrestrial ecosystems of the Eastern Mediterranean region associated with the 8.2 kyr B.P. climatic event, *Geology*, *37*, 887–890, doi:10.1130/G25739A.1.
Pujol, C., and C. Vergnaud-Grazzini (1995), Distribution patterns of live planktic foraminifers as related to regional hydrography and productive systems of the Mediterranean Sea, *Mar. Micropaleontol.*, *25*, 187–217, doi:10.1016/0377-8398(95)00002-I.
Ramsey, C. B. (2009), Bayesian analysis of radiocarbon dates, *Radiocarbon*, *51*, 337–360, doi:10.2458/azu_js_rc.51.3494.
Reimer, P. J., et al. (2009), IntCal09 and Marine09 radiocarbon age calibration curves, 0–50,000 years cal BP, *Radiocarbon*, *51*, 1111–1150.
Reiss, Z., E. Halicz, and B. Luz (1999), Late Holocene foraminifera from the SE Levantine Basin, *Isr. J. Earth Sci.*, *48*, 1–17.
Revel, M., E. Ducassou, F. E. Grousset, S. M. Bernasconi, S. Migeon, S. Revillon, J. Mascle, A. Murat, S. Zaragosi, and D. Bosch (2010), 100,000 years of African monsoon variability recorded in sediments of the Nile margin, *Quat. Sci. Rev.*, *29*, 1342–1362, doi:10.1016/j.quascirev.2010.02.006.
Revel, M., et al. (2014), 21,000 years of Ethiopian African monsoon variability recorded in sediments of the western Nile deep-sea fan, *Reg. Environ. Change*, *1–12*, doi:10.1007/s10113-014-0588-x.

Roberts, N., et al. (2012), Palaeolimnological evidence for an east–west climate see-saw in the Mediterranean since AD 900, *Global Planet. Change*, *84–85*, 23–34, doi:10.1016/j.gloplacha.2011.11.002.
Robinson, S. A., S. Black, B. W. Sellwood, and P. J. Valdes (2006), A review of palaeoclimates and palaeoenvironments in the Levant and Eastern Mediterranean from 25,000 to 5000 years BP: Setting the environmental background for the evolution of human civilization, *Quat. Sci. Rev.*, *25*, 1517–1541, doi:10.1016/j.quascirev.2006.02.006.
Rohling, E. J. (1994), Review and new aspects concerning the formation of eastern Mediterranean sapropels, *Mar. Geol.*, *122*, 1–28, doi:10.1016/0025-3227(94)90202-X.
Rohling, E. J., and H. Pälike (2005), Centennial-scale climate cooling with a sudden cold event around 8,200 years ago, *Nature*, *434*, 975–979, doi:10.1038/nature03421.
Rohling, E. J., and W. W. C. Gieskes (1989), Late Quaternary changes in Mediterranean intermediate water density and formation rate, *Paleoceanography*, *4*, 531–545, doi:10.1029/PA004i005p00531.
Rohling, E. J., F. J. Jorissen, C. V. Grazzini, and W. J. Zachariasse (1993), Northern Levantine and Adriatic Quaternary planktic foraminifera; reconstruction of paleoenvironmental gradients, *Mar. Micropaleontol.*, *21*, 191–218, doi:10.1016/0377-8398(93)90015-P.
Rohling, E. J., et al. (2004), Reconstructing past planktic foraminiferal habitats using stable isotope data: A case history for Mediterranean sapropel S5, *Mar. Micropaleontol.*, *50*, 89–123, doi:10.1016/S0377-8398(03)00068-9.
Rossignol-Strick, M. (1995), Sea-land correlation of pollen records in the Eastern Mediterranean for the glacial-interglacial transition: Biostratigraphy versus radiometric time-scale, *Quat. Sci. Rev.*, *14*, 893–915, doi:10.1016/0277-3791(95)00070-4.
Rossignol-Strick, M., W. Nesteroff, P. Olive, and C. Vergnaud-Grazzini (1982), After the deluge: Mediterranean stagnation and sapropel formation, *Nature*, *295*, 105–110, doi:10.1038/295105a0.
Rouis-Zargouni, I., J.-L. Turon, L. Londeix, L. Essallami, N. Kallel, and M.-A. Sicre (2010), Environmental and climatic changes in the central Mediterranean Sea (Siculo–Tunisian Strait) during the last 30 ka based on dinoflagellate cyst and planktonic foraminifera assemblages, *Palaeogeogr. Palaeoclimatol. Palaeoecol.*, *285*, 17–29, doi:10.1016/j.palaeo.2009.10.015.
Saji, N. H., B. N. Goswami, P. N. Vinayachandran, and T. Yamagata (1999), A dipole mode in the tropical Indian Ocean, *Nature*, *401*, 360–363, doi:10.1038/43854.
Sbaffi, L., F. C. Wezel, N. Kallel, M. Paterne, I. Cacho, P. Ziveri, and N. Shackleton (2001), Response of the pelagic environment to palaeoclimatic changes in the central Mediterranean Sea during the late Quaternary, *Mar. Geol.*, *178*, 39–62, doi:10.1016/S0025-3227(01)00185-2.
Schilman, B., M. Bar-Matthews, A. Almogi-Labin, and B. Luz (2001), Global climate instability reflected by Eastern Mediterranean marine records during the late Holocene, *Palaeogeogr. Palaeoclimatol. Palaeoecol.*, *176*, 157–176, doi:10.1016/S0031-0182(01)00336-4.
Schilman, B., A. Ayalon, M. Bar-Matthews, E. J. Kagan, and A. Almogi-Labin (2002), Sea-land paleoclimate correlation in the Eastern Mediterranean region during the late Holocene, *Isr. J. Earth Sci.*, *51*, 181–190, doi:10.1560/504G-007U-5NKY-GUN1.
Schilman, B., A. Almogi-Labin, M. Bar-Matthews, and B. Luz (2003), Late Holocene productivity and hydrographic variability in the Eastern Mediterranean inferred from benthic foraminiferal stable isotopes, *Paleoceanography*, *18*, 9.1–9.12, doi:10.1029/2002PA000813.
Schmidt, D. N., S. Renaud, J. Bollmann, R. Schiebel, and H. R. Thierstein (2004a), Size distribution of Holocene planktic foraminifer assemblages: Biogeography, ecology and adaptation, *Mar. Micropaleontol.*, *50*, 319–338, doi:10.1016/S0377-8398(03)00098-7.
Schmidt, D. N., H. R. Thierstein, J. Bollmann, and R. Schiebel (2004b), Abiotic forcing of plankton evolution in the Cenozoic, *Science*, *303*, 207–210, doi:10.1126/science.1090592.
Schmiedl, G., A. Mitschele, S. Beck, K.-C. Emeis, C. Hemleben, H. Schulz, M. Sperling, and S. Weldeab (2003), Benthic foraminiferal record of ecosystem variability in the Eastern Mediterranean Sea during times of sapropel S5 and S6 deposition, *Palaeogeogr. Palaeoclimatol. Palaeoecol.*, *190*, 139–164, doi:10.1016/S0031-0182(02)00603-X.
Schmuker, B., and R. Schiebel (2002), Planktic foraminifers and hydrography of the eastern and northern Caribbean Sea, *Mar. Micropaleontol.*, *46*, 387–403, doi:10.1016/S0377-8398(02)00082-8.
Singh, G., R. J. Wasson, and D. P. Agrawal (1990), Vegetational and seasonal climatic changes since the last full glacial in the Thar Desert, northwestern India, *Rev. Palaeobot. Palynol.*, The Proceedings of the 7th International Palynological Congress (Part I), *64*, 351–358, doi:10.1016/0034-6667(90)90151-8.
Spero, H. J., I. Lerche, and D. F. Williams (1991), Opening the carbon isotope "vital effect" black box, 2, Quantitative model for interpreting foraminiferal carbon isotope data, *Paleoceanography*, *6*, 639–655, doi:10.1029/91PA02022.
Toker, E., D. Sivan, E. Stern, B. Shirman, M. Tsimplis, and G. Spada (2012), Evidence for centennial scale sea level variability during the Medieval Climate Optimum (Crusader Period) in Israel, Eastern Mediterranean, *Earth Planet. Sci. Lett.*, *315–316*, 51–61, doi:10.1016/j.epsl.2011.07.019.
Ufkes, E., J. H. Fred Jansen, and G.-J. A. Brummer (1998), Living planktonic foraminifera in the eastern South Atlantic during spring: Indicators of water masses, upwelling and the Congo (Zaire) River plume, *Mar. Micropaleontol.*, *33*, 27–53, doi:10.1016/S0377-8398(97)00032-7.
UNEP/MAP (2012), *State of the Mediterranean Marine and Coastal Environment*, Barcelona Convention, Athens.
Van der Plas, L., and A. C. Tobi (1965), A chart for judging the reliability of point counting results, *Am. J. Sci.*, *263*, 87–90, doi:10.2475/ajs.263.1.87.
Wang, L. (2000), Isotopic signals in two morphotypes of *Globigerinoides ruber* (white) from the South China Sea: Implications for monsoon climate change during the last glacial cycle, *Palaeogeogr. Palaeoclimatol. Palaeoecol.*, *161*, 381–394, doi:10.1016/S0031-0182(00)00094-8.
Wanner, H., et al. (2008), Mid- to late Holocene climate change: An overview, *Quat. Sci. Rev.*, *27*, 1791–1828, doi:10.1016/j.quascirev.2008.06.013.
Weldeab, S., V. Menke, and G. Schmiedl (2014), The pace of East African monsoon evolution during the Holocene, *Geophys. Res. Lett.*, *41*, 1724–1732, doi:10.1002/2014GL059361.
Williams, M. A. J., J. N. Pal, M. Jaiswal, and A. K. Singhvi (2006), River response to Quaternary climatic fluctuations: Evidence from the Son and Belan valleys, north-central India, *Quat. Sci. Rev.*, *25*, 2619–2631, doi:10.1016/j.quascirev.2005.07.018.
Wüst, G. (1961), On the vertical circulation of the Mediterranean Sea, *J. Geophys. Res.*, *66*, 3261–3271, doi:10.1029/JZ066i010p03261.
Xoplaki, E., J. F. Gonzalez-Rouco, J. Luterbacher, and H. Wanner (2004), Wet season Mediterranean precipitation variability: Influence of large-scale dynamics and trends, *Clim. Dyn.*, *23*, 63–78, doi:10.1007/s00382-004-0422-0.
Zonneveld, K. A. F., G. J. M. Versteegh, and G. J. de Lange (2001), Palaeoproductivity and post-depositional aerobic organic matter decay reflected by dinoflagellate cyst assemblages of the Eastern Mediterranean S1 sapropel, *Mar. Geol.*, *172*, 181–195, doi:10.1016/S0025-3227(00)00134-1.